Single Photon Imaging System for the ESS Linac

Maria Hoflund

Department of Electrical and Information Technology
Lund University

Supervisors: Cyrille Thomas (ESS) and Anders Karlsson (LTH)

Examiner: Mats Gustafsson

September 17, 2019

Printed in Sweden
Tryckeriet i E-huset, Lund

Abstract

To control an accelerating proton beam that travels close to the speed of light, a large number of beam diagnostic instruments are needed. One of the instruments that will be used at the accelerator of the European Spallation Source is a Non-invasive Profile Monitor (NPM). Once installed, this system will measure the transverse beam profile by imaging the fluorescent gas induced by the accelerated proton beam. However, there are two problems that make this system more complex than just using a camera. In the Medium Energy Beam Transport (MEBT) section where this monitor is going to be placed, the light intensity will be very low. The NPM has to image the beam in a single photon counting mode. To achieve this, an image intensifier is used to amplify the number of photons. The second problem is the high level of radiation next to the beam. The camera has to be placed in a shielded area away from the beam, and the image is therefore transported via a 10-meter-long fiber bundle to the camera. The goal of this thesis is to understand the characteristics of the NPM and to demonstrate that single photon imaging is possible. The results show that these requirements are fulfilled if some suggested modifications are made. An additional model of the system was implemented in MATLAB, to understand its response when parameters of the system are varied. The work of this thesis, including the model, can be used when designing future systems similar to the NPM.

Acknowledgement

I would like to express my great appreciation to my supervisor Cyrille Thomas, who has generously given me a lot of time to support me throughout this thesis. His valuable inputs, directions, discussions and knowledge have helped me to develop as a researcher. I am also grateful that I could contribute to his project. I would also like to thank my supervisor from LTH, Professor Anders Karlsson, who has given me helpful feedback during this work. It has been very useful for me to discuss my progress with Anders, who had a bird's eye view of the project. I would also like to thank the rest of the beam diagnostic group at ESS. A special thanks to Thomas Shea, who has been keeping an eye on me, during the project, to make sure that I had all the help I needed. He was also contributing with fruitful discussions that helped the work move forward. I would also like to thank Roxana Tarkeshian, who has helped me with discussions and answered various questions that I have had. I would also like to thank Hinko Kocevar, who helped me to set up the input output controls for the different devices that were used in the lab. His work enabled the measurements to be very efficient. The amount of work that was done during this period, would not be as large without his help. Lastly, I would also like to thank Peter van Velze, who taught me how to mount and polish the fiber connectors.

Popular Science Summary

Photographing a Proton Beam

How do you take a picture of an accelerating proton beam? Is it even possible? And why would you want to? To steer protons at close to the speed of light you need to see what you are doing. As it turns out, a good camera and a bit of fluorescent light makes this a possibility.

At the European Spallation Source (ESS), protons will be accelerated to 96 % of the speed of light. These highly energetic protons will then collide with bigger atoms and a burst of neutrons are released. This process is called neutron spallation, which explains the name of ESS. These neutrons can then be used for studying all kinds of materials.

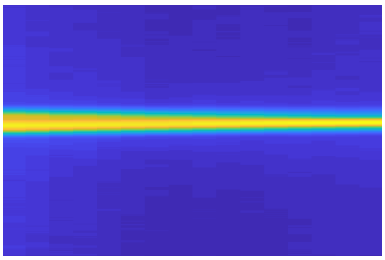

Image of the ESS-proton beam taken with a Non-invasive Profile Monitor.

Along the accelerator, there are lots of instruments that provide information about the proton beam. One important characteristic is the transverse beam profile. This can be measured by taking a picture of beam-induced-fluorescence. As the protons race down the beam pipe, they interact with residual hydrogen gas. When the gas gets excited, it emits photons. This process is called fluorescence; it is caused by protons lighting up the gas. But the gas will only shine where the beam is present, which is how its shape can be detected. The figure shows a real picture taken of this glow induced by the protons.

At some parts of the accelerator, the density of gas is very low, which makes the light intensity low too. A very sensitive instrument is required to detect something as dim as a single photon of light. In the work of this thesis, an instrument called a Non-invasive Profile Monitor is prototyped and it has demonstrated the possibility of detecting such low intensities of light.

Table of Contents

List of Abbreviations

BP	Band-Pass
BS	Beam Splitter
CCD	Charge-Couple Device
CMOS	Complementary Metal Oxide Semiconductor
EPICS	Experimental Physics and Industry Control System
ESS	European Spallation Source
FPM	Fluorescence Profile Monitor
IOC	Input Output Controller
LED	Light Emitting Diode
Linac	Linear Accelerator
MCP	Microchannel Plate
MTF	Modulation Transfer Function
NPM	Non-invasive Profile Monitor
PSF	Point Spread Function
QE	Quantum Efficiency
SNR	Signal to Noise Ratio

Chapter 1
Introduction

The European Spallation Source (ESS) is a neutron source that is under construction in the vicinity of Lund, Sweden. The neutron source works like a big microscope. It can be used to study small structures in materials down to the atomic level. Compared to a microscope, which uses photons to detect, ESS uses neutrons. Neutrons interact with materials in different ways, making it possible to see new things which can not be seen with light. When the construction of ESS is finished, in 2023, scientists from a broad range of fields will come here to put their samples in one of the fifteen different instruments distributed around the neutron source. Every instrument will use the neutrons in their own way to perform different kinds of measurements such as: diffraction, spectroscopy, reflectometry and imaging. ESS's specialty will be long pulses with high intensity. This comes with several benefits for the scientists using the source.

At the European Spallation Source, as the name reveals, neutrons are generated through a spallation process. This process takes place when highly energetic protons collide with a target, in this case a heavy metal. The target's nuclei are excited by the protons and emit a large number of neutrons through relaxation. To get these highly energetic protons, they are first generated from an ion source. In the ion source, hydrogen gas is heated up to a high temperature to make a plasma. In a plasma, the electrons and protons of the atoms are separated and the protons can be extracted. The protons gain energy along a 500 meter linear accelerator. The accelerator is designed to generate protons with an energy of 2 GeV. The protons come in pulses of 2.86 ms with a repetition rate of 14 Hz. The average power will be 5 MW and the peak power will be 125 MW. While being accelerated, the proton beam has to be kept small and straight, and the bunches need to keep the right length. Magnets are therefore used to control and steer the protons. Just like driving a car, you need to see where you are driving to be able to steer in the right direction. In the accelerator the driver will see where the beam is going with the help of all the beam diagnostic instruments distributed along the accelerator. These instruments are crucial to get the required properties of the beam when it hits the target. They have to be accurate and give all the necessary information about the beam to make it possible to control it. Properties of the beam that can be measured are for example: beam current, beam position, emittance, pulse length, beam loss and beam profile.

The topic of this master's thesis is one of these beam profile monitors. This monitor measures the transverse beam profile with an optical imaging system.

Thanks to the interaction between protons and residual gas in the tube, the beam's presence is spotted by fluorescence. Taking a picture of this will reveal the profile of the beam. This beam diagnostic is called a Non-invasive Profile Monitor (NPM), at ESS. The intensity of the fluorescent light is proportional to the density of residual gas and the number of protons interacting. The cross section for interaction is higher when the protons have a low energy. In the beginning of the accelerator, the gas pressure and the cross section for interaction are relatively high. The light is intense enough so that a standard camera can be placed just next to the beam and pictures can be taken of it. Further away from the ion source, the gas pressure is lower and the cross section has dropped about three orders of magnitude. To be able to detect the beam profile at this position, the detector needs to be in a single photon counting mode. Furthermore, this detector will be placed in a radioactive environment that would damage the camera. Therefore the image has to be transported via a fiber to a less exposed area where the camera can detect the image.

A design of this NPM had been proposed by Cyrille Thomas, prior to this master's thesis. The goal of this thesis is to demonstrate how the system works, based on this design, and to evaluate if it can detect single photons. Some features that are investigated include resolution, noise, saturation, gain and losses. The goal of the characterization is to find limitations and possible improvements of the performance of the NPM.

The thesis is divided into five chapters. This introduction is the first chapter. Chapter 2 introduces the theoretical background of the beam induced fluorescence, the different parts of the system, optics, and imaging systems. The third chapter describes how the system was characterized and the results of that. The characterization of every part of the system has its own section. In every section, the method, results, and analysis are presented. The fourth chapter describes a simulation model that has been developed to understand the NPM. From this model, some improvements of the system were suggested. The last chapter contains a discussion that summarizes and analyses the main results.

Chapter 2

Theoretical Background

2.1 Beam Induced Fluorescence

Beam induced fluorescence is a phenomenon that makes it possible to measure the transverse beam profile non-invasively. When protons are accelerated through the close-to-vacuum tube, they interact with the residual gas in the tube. The position where this monitor is going to operate is called the Medium Energy Beam Transport (MEBT). The pressure in this section of the accelerator is $p = 10^{-5}$ - 10^{-6} Pa [1]. The gas contains 63 % - 80 % H_2, and the rest is CO, CO_2, CH_4, Ar and H_2O [2]. To estimate the number of fluorescent photons, the gas is assumed to only contain H_2.

Before the fluorescent process can be explained, the following question has to be answered: what is a photon? Light can be understood both as a wave and a particle. In some experiments, light has wave-like behavior and in other experiments it has particle-like behavior. This double-perspective is called the wave-particle duality. The light particle is called a photon. It is a massless, neutral particle with an energy associated with its wavelength. It can be seen as an energy packet of light. When a photon interacts with an atom, the energy is either completely absorbed or not absorbed at all. The energy cannot be divided into fractions. Light is said to be quantized.

When a proton collides with a H_2 molecule, a fluorescent photon can be emitted from the excited molecule. There is a probability that one of the electrons absorbs some of the energy from the proton and goes into an excited state of the molecule. After the electron has been excited, it decays down to the ground state again. It can take different paths through the possible states. When a transition from a higher energy state to a lower energy state occurs, a photon is emitted. The photon has the same energy as the energy difference between the states. Different decay transitions have different probabilities due to the properties of the hydrogen molecule. Measurements have shown that the hydrogen molecules mainly emit at the Blamer-α spectral line [3]. It has a wavelength of 656 nm and originates from the transition between n = 3 and n = 2, where n is the principal quantum number of the state. The probability for the whole process of exciting an electron and of a Balmer-α photon to be emitted can be summarized in one cross section, σ. For the 3.6 MeV protons, this cross section was estimated to 10^{-18}cm^2 from the results of J. G. Lodge et al. and using the Bethe formula [4].

The protons are accelerated in pulses. The number of protons per pulse can be estimated from the current and the pulse length. In the MEBT, the current is $I_b = 62.5\,mA$ and the pulse length is $t = 2.86\,ms$ [1]. The estimated number of photons per pulse, N_{ph}, is derived in Equation (2.1), where N_{pr} is the number of protons per pulse, e is the elementary charge, N_{H_2} is the number of hydrogen molecules (calculated with the ideal gas law), N_A is the Avogadro constant, R is the gas constant, and T is the temperature. The photons are emitted in all directions from the beam. Only a fraction ($\sim 10^{-4}$) are captured by the lens.

$$\begin{aligned} N_{pr} &= I_b \cdot t/e = 62.5 \cdot 10^{-3} \cdot 2.86 \cdot 10^{-3}/1.6 \cdot 10^{-19} = 1.1172 \cdot 10^{15} \\ N_{H_2} &= N_A \cdot p/(R \cdot T) = 6 \cdot 10^{23} \cdot 10^{-6}/(8.3145 \cdot 300) \cdot 10^{-6} = 2.4054 \cdot 10^{8} \mathrm{cm}^{-3} \\ N_{ph} &= N_{pr} \cdot N_{H_2} \cdot \sigma = 1.1172 \cdot 10^{15} \cdot 2.4054 \cdot 10^{8} \cdot 10^{-18} = 2.6874 \cdot 10^{5} \mathrm{cm}^{-1} \end{aligned} \tag{2.1}$$

2.2 The Non-invasive Profile Monitor

The Non-invasive Profile Monitor, or the Fluorescence Profile Monitor (FPM) as it sometimes is called, is already a standard diagnostic tool at other accelerator facilities around the world. They take different forms, however, depending on the circumstances at each facility. A non-invasive monitor means that it is not disturbing the beam and it can be used for high beam currents. Invasive monitors, like wire scanners, run a high risk of being damaged when the beam power is large [5]. Wire scanners are more sensitive and therefore more suitable for low beam currents. Typically, wire scanners are used while tuning the accelerator machine and the NPM can be used when the machine is running at full power [6]. There is no instrument that works in all conditions, which is why different types are needed to complement each other.

The general design of a NPM has an imaging system that detects the fluorescent light from the beam onto a camera sensor. Due to different circumstances of the light source, and the level of radiation at the location of the system, the design can vary at different facilities. When the light source is under the detectable threshold of the camera, the image has to be intensified. This can be achieved with a separate device in front of the camera or an integrated amplification system in the camera. If the radiation level is high, the camera has to be radiation hard, shielded, or placed in another room.

A sketch of the NPM that is going to be installed in the ESS linear accelerator (linac) is shown in Figure 2.1. Due to the low number of photons, it has a separate device that amplifies the light intensity. This device is called an image intensifier and is described in the next section. The first element in the system is a lens, L1, that images the beam onto the image intensifier. After the image has been intensified, it is imaged with a lens, L2, and transported by a fiber bundle away from the accelerator. This is necessary for protecting the camera from the radiation around the accelerator. A third lens, L3, then images the fiber output onto the camera sensor. The camera is connected to a computer that can analyze and display the signal.

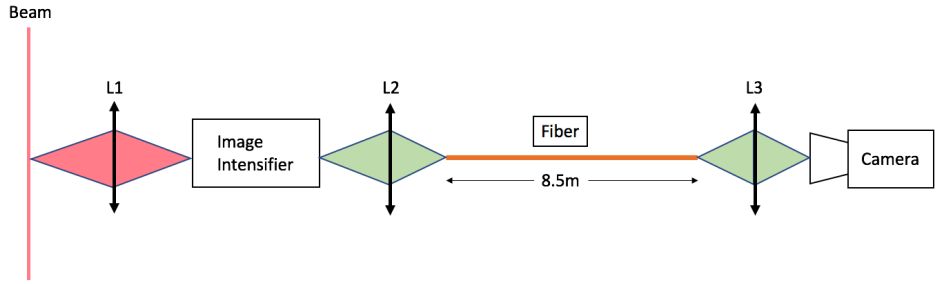

Figure 2.1: A simple sketch showing the main components of the imaging system. "Beam" refers to the proton beam that is going to be imaged. L1, L2 and L3 are three different lens systems that are imaging between the different components. The image intensifier is intensifying the image. The fiber is a fiber bundle of 13000 fibers that transports the image to a less radioactive area. The camera is detecting the image so that it can be analyzed and displayed. The red and green cones represent the color of the light captured by the lenses.

2.3 The Image Intensifier

An image intensifier is an opto-electronic device that amplifies the intensity of a faint image [7]. This is based on the photoelectric effect that Einstein explained in 1905 and got the Nobel Prize in physics for in 1921 [8]. The following explanation of how it works is taken from Michael Lampton [7]. A photon can be converted into an electron, also called a photoelectron. If the energy of the photon is large enough to release an electron from an atom the photon is absorbed and effectively converted into a free electron. This effect is used in both the image intensifier and its predecessor, the electron multiplier. When the photons are converted into electrons, the number of electrons are amplified and then converted back into photons again.

The photoelectric effect takes place in something called a photocathode. The cathode has a negative potential which creates a repulsion of the free photoelectrons. In the electron multiplier, the electrons are attracted towards a dynode which is a metal electrode with a positive voltage. When the electron hits the dynode, secondary electrons are released and all of the electrons are accelerated to the next dynode that has an even higher positive voltage. This goes on until the last dynode. The number of electrons are multiplied at every dynode which gives an exponential growth of electrons. At the back of the electron multiplier, there is a fluorescent screen. It works like a reverse photocathode. It emits photons when being hit by electrons. The result is a multiplication of photons emitted from the fluorescent screen compared to the number of incoming photons.

The image intensifier is like an electron multiplier but with an additional spatial resolution. Instead of having one "channel", where the number of electrons are multiplied, the image intensifier has a two dimensional array of microchannels. Every channel acts like a pixel. This makes the image intensifier not only capable

of intensifying the light, but also of containing the spatial information of an image. A picture of an image intensifier is shown in Figure 2.2. Just like the electron multiplier, the incoming photons hit a photocathode that emits electrons. The electrons are accelerated towards the microchannel plate (MCP) by an applied voltage. Each electron enters one of the channels. It accelerates through the channel by an additional applied voltage over the MCP. When it travels through the channel, it hits the walls and secondary electrons are released, just like the dynodes in the electron multiplier. At the end of each channel, a multiplication of the incoming number of electrons are exiting. All these electrons are then accelerated towards the fluorescent screen. It emits a number of photons per electron. The number depends on the type of material and the kinetic energy of the electrons. The result is an intensified version of the incoming image.

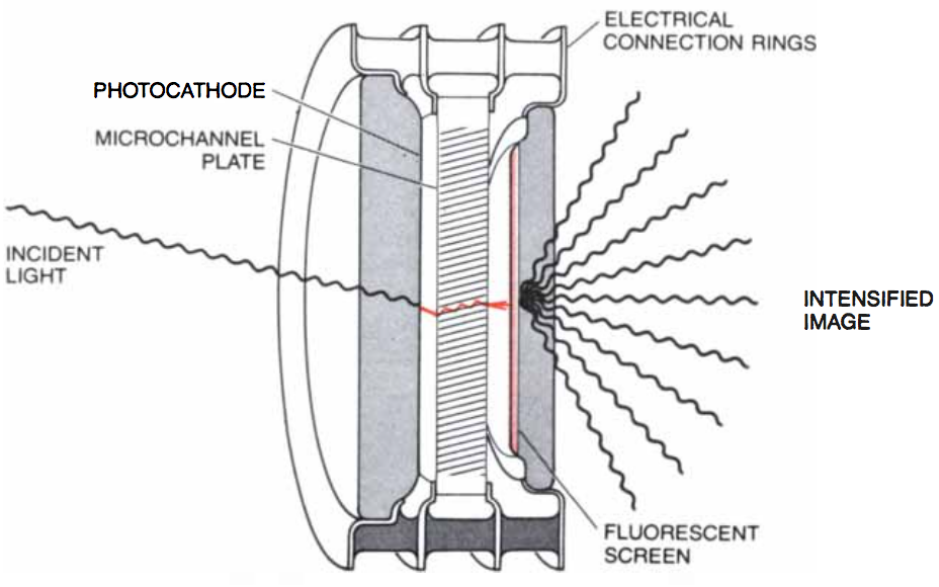

Figure 2.2: A sketch of an image intensifier. The figure is taken from M. Lampton [7].

The multiplication factor of the MCP, also called the gain, can be varied by varying the applied voltage over the MCP. A higher voltage gives the electrons a higher kinetic energy. A higher kinetic energy releases more secondary electrons from the walls [9]. This gives a larger number of electrons at the output of the MCP. The number of electrons generated from each interaction with the wall is a function of the number of incoming electrons. The number of electrons is therefore an exponential function of distance in the channel. The gain as a function of applied voltage is also an exponential function. However, there are other effects that cause saturation for higher voltages and higher input signals. Saturation occurs from space charge and dead time effects [10]. In the walls of each channel, there is a strip current. When secondary electrons are released from the walls, the strip current recovers the absence of these electrons. If there is a high gain or

large input signal, there is a large number of electrons in the end of the channel. A large number of electrons are also released from the walls. Since the current is not instant, there is a "dead time" until the strip current has recovered the wall and more electrons can be released. Additionally, when a lot of electrons are generated in the end of the channel they suppress the electric field, due to their own charge and this lowers the acceleration. This is called the space charge effect. To increase the gain further than the applied voltage is able to, the amplification can be done in several stages.

The image intensifier that was used in this project is manufactured by Photonis. It has a single-stage MCP. They typically have a gain of approximately 10^4 for an applied voltage of 1 kV [10]. The photocathode type is S20. The light that is detected has a peak at the wavelength 656 nm. The S20 photocathode has a quantum efficiency around 5 % at this wavelength [11]. This means that for every 100 incoming photons, there is about 5 electrons emitted from the photocathode. The usable diameter of the input window is 17.5 mm. The fluorescent material on the back is a P46 phosphor screen. It has a relatively short decay time, 0.2 µs [12], it emits about 6 ph /(el · kV) [10] and has a peak emission wavelength at 510 nm [10]. At the back of the phosphor screen, there is a fiber optic plate with a taper attached. The fiber optic plate is a bundle of fibers that transports the image with low distortion. The taper is an extension which demagnifies the image, 1:2.19, with an output area of 4.9 x 6.5 mm. In Figure 2.3, one can see the fiber optic plate with the taper sticking out of the black cylinder. The taper transforms the circular surface into a square. This means that some parts of the image and some light intensity is lost.

Figure 2.3: A figure of the image intensifier, taken from the Photonis data sheet [13]. It shows the geometry of the fiber optic plate with the taper sticking out of the black cylinder.

2.4 The Imaging Fiber

Light is difficult to transport long distances without losing intensity. This changed in 1841 when Daniel Colladon accidentally discovered that light can be guided and bent in a stream of water exiting a water tank [14]. The basis of optical fibers was discovered, but it took 168 years until Charles K. Kao got the Nobel Prize in Physics “for groundbreaking achievements concerning the transmission of light in fibers for optical communication” as stated by the Royal Swedish Academy of Science [15]. The optical fiber transports light through a very thin glass core.

The fiber can be bent and directed wherever you want the light, with low losses. The physical phenomenon that enables the guidance of light through the fiber is refraction. Light is refracted when it propagates from one material with one index of refraction into another material with another index of refraction. It changes its direction of propagation according to Snell's law. If the first material has a higher index of refraction than the second material, the light bends from the perpendicular. If the incident angle is large enough, the refractive angle is 90° or higher. In that case the light does not enter the second medium, and all of the light is reflected at the interface. This is called total internal reflection and this is how the light is guided through the fiber. A sketch of the light path through a fiber is shown in Figure 2.4.

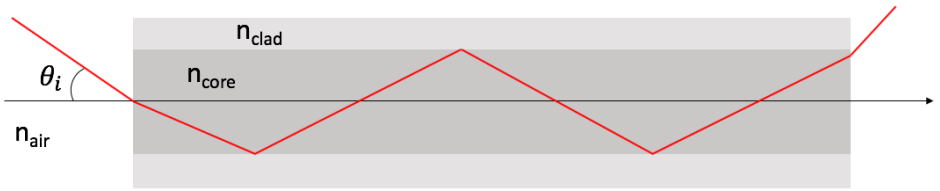

Figure 2.4: This figure shows the essential parts of an optical fiber. Light enters the fiber with an incident angle, θ_i. It gets refracted, due to the difference in refractive index between air, n_{air}, and the core material, n_{core}. The light is reflected at the interfaces to the cladding, by total internal reflection. The refractive index of the cladding, n_{clad}, has to be smaller than the core. The cross section of the fiber is usually circular.

The fiber consist of a core with an index of refraction n_{core} and a cladding with an index of refraction n_{clad}, where n_{core} is larger than n_{clad}. If the incident angle, θ_i, is too large, there will not be total internal reflection. Therefore every fiber has a maximum acceptable incident angle. This is usually expressed in a numerical aperture defined by Equation (2.2). The right side of the equation is derived from Snell's law, and is valid for multimode fibers.

$$NA = \sin(\theta_i) = \sqrt{{n_{core}}^2 - {n_{clad}}^2} \tag{2.2}$$

The fiber that is used in this project is an imaging fiber. It is a bundle of 13000 fiber cores in one fiber, similar to the fiber optical plate mentioned in the previous section. Every fiber core acts like a channel, or a pixel, and it can therefore transport a two dimensional image. This fiber bundle is manufactured by Asahi Kasei, and the model is MBL. It has a diameter of 1.5 mm and a numerical aperture of 0.5. The core material is made of PMMA (Polymethyl methacrylate), also known as acrylic glass or plexiglass, and the cladding material is Fluorinated Polymer.

Even if the light undergoes total internal reflection, its intensity is attenuated by absorption and scattering in the material. It is strongly dependent on the material but also the wavelength of the light. The power of light through the fiber decreases exponentially with the length of the fiber. The attenuation as a function

of wavelength for this fiber is shown in Figure 2.5. The wavelength of the light that propagates through the fiber is around 510 nm. There are also losses from the coupling of light into the fiber, due to reflection at the surface and because of the spacing between the cores. The power at the output of a fiber can be described by Equation (2.3), where P_{out} is the output power, P_{in} is the input power, C is the coupling efficiency, L is the length of the fiber and α is the attenuation coefficient (per length unit) [16].

$$P_{out} = P_{in} \cdot C \cdot e^{-\alpha L} \tag{2.3}$$

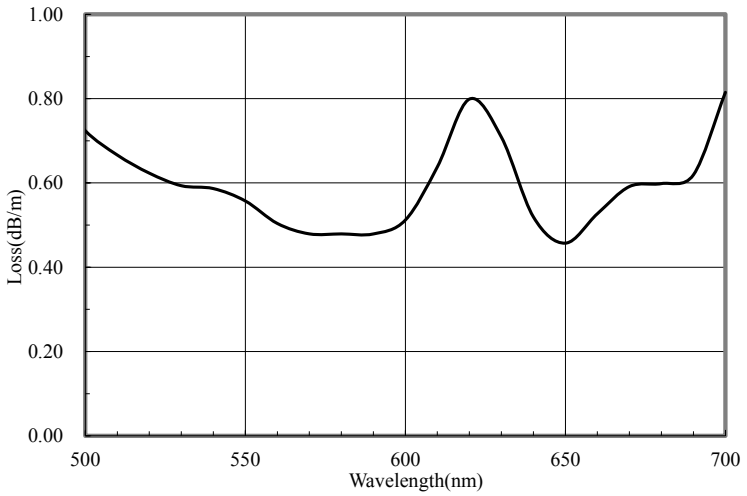

Figure 2.5: Attenuation as a function of wavelength for the Asahi Kasei MBL-2000 imaging fiber [17].

2.5 The Digital Camera

The same year as Charles K. Kao got the Nobel Prize in physics for the optical fiber, Willard S. Boyle and George E. Smith got the other half of the same prize for the invention of the CCD sensor, which is the basis of the digital camera. In a digital camera, each pixel contains a photodiode [18]. The photodiode can absorb photons with a certain probability, called quantum efficiency. The quantum efficiency is wavelength dependent. For every photon that is absorbed, an electron is excited to the conduction band. The electrons are accumulated for a certain time, called the exposure time, when the photodiode is forward biased. When the bias is turned off, a voltage has been built up by the excited electrons and is then read out by an analog to digital converter. The output from the camera is a digital number for each pixel. Most cameras today have a different sensor called CMOS, short for Complementary Metal Oxide Semiconductor [19]. The difference between the two sensors is that the CCD has one place where the voltage is read

out while the CMOS has read-out-electronics at each pixel. The camera used in this project has a CMOS sensor.

To explain the properties of a digital camera the simplified model in Figure 2.6 is used. It describes the process going from a number of incoming photons to a digital number at the output, for each pixel. A number of photons, μ_p, hit the photodiode. The quantum efficiency, η, describes the probability that each photon converts into an electron [18]. Statistically, this can be seen as a Poisson distribution. The noise from this process is called photon noise, or shot noise. It comes from the quantized nature of light and can never be suppressed. If $\mu_e = \eta \cdot \mu_p$ is the mean number of electrons, the photon noise is: $\sigma_e = \sqrt{\mu_e}$ [18]. Distinct from the electrons that are generated from the absorption of a photon, are additional electrons, called dark electrons, or dark current. In the photodiode, dark electrons can be excited due to thermal energy. This happens independently of the incoming light, which is why they are called dark electrons. The longer the exposure time, the more dark electrons are accumulated. There is always a variation in the number of dark electrons, this is called the dark noise, σ_d. The next step is to convert the number of electrons into a digital number. The conversion factor is called the system gain, K, and is dependent on how the analog-to-digital converter is designed. Since the digital values only can take discrete steps, there is quantization noise, σ_q, from this process. After all these steps, there is an output in terms of a digital grey value for each pixel. The responsivity, R, of the camera, defines the average digital value from one incoming photon. The responsivity is also the product of the quantum efficiency and the system gain.

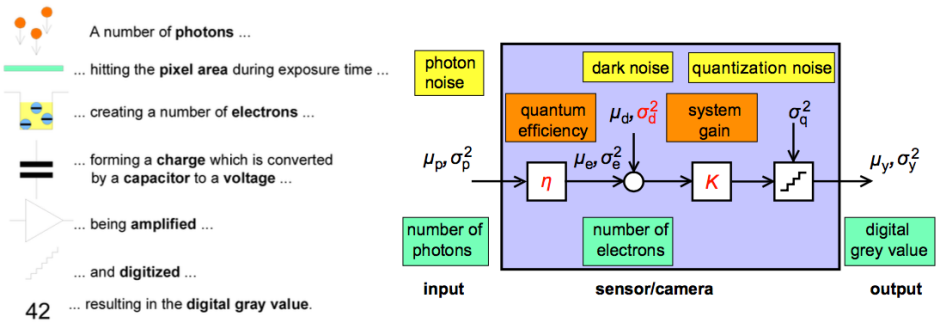

Figure 2.6: A model of a digital camera. The left side of the figure describes the process for detecting a number of photons in a pixel. The right side of the figure shows all the parameters that affect the output value as a function of input. The figure is taken from the EMVA Standard 1288 [18].

A camera sensor has a minimum and maximum number of photons that can be detected by each pixel. The minimum detectable number is defined by the noise. When the signal is larger than the noise, it is considered to be detectable [18]. That is the same as saying that the SNR (signal-to-noise ratio) has to be greater than one. The SNR is defined by Equation (2.4), where μ_y is the pixel value, $\mu_{y.dark}$ is the dark pixel value and σ_y is the noise per pixel. The maximum

number of photons that can be detected is limited by a physical saturation level in the photodiode. There is also a maximum digital value that normally is set to be lower than the physical maximum. For a 12-bit sensor, the maximum digital value is $2^{12} = 4096$. If a pixel is showing this value, it is said to be saturated.

$$\mathrm{SNR} = \frac{\mu_y - \mu_{y.dark}}{\sigma_y} \tag{2.4}$$

The camera used in this project is a MAKO G-234. Some of the properties of the camera are listed in Table 2.1.

Table 2.1: Properties of the MAKO G-234 [20].

Resolution	1936 x 1216
Sensor type	CMOS
Sensor size	Type 1/1.2
Pixel size	5.86 µm x 5.86 µm
ADC	12 bit

2.6 Optical Imaging

Between each component of the NPM, there is a lens system. This section describes the imaging equations that are necessary for understanding optical imaging. Furthermore, the optical throughput is discussed and lastly the method of measuring resolution.

2.6.1 Imaging equations

A simple optical imaging system consists of a lens that refracts the light from an object to form an image. A lens can focus (convex) or disperse (concave) the rays [21]. It is made of transparent material such as glass or plastic. A common lens is the spherical lens. It has spherically shaped surfaces and a focal length, f, defined by the radius of curvature. The focal length is the distance from the lens where all rays that are parallel to the optical axis are focused. The imaging Equation (2.5) connects the distance from the object to the lens, s, to the distance from the lens to the image, s', as a function of the focal length. Two approximations have been made in this equation. The lens is assumed to be thin and the rays are assumed to be paraxial. A paraxial ray is a ray that has a small angle, θ, to the optical axis. Assuming this, the following approximations can be make: $\sin\theta \approx \theta$, $\tan\theta \approx \theta$ and $\cos\theta \approx 1$.

$$\frac{1}{s} + \frac{1}{s'} = \frac{1}{f} \tag{2.5}$$

Figure 2.7 shows an example of a convex lens that images a point (s, y) to the point (s', y'). The scaling factor between the object and image is called the

system's magnification, m, given by Equation (2.6).

$$y' = -\frac{s'}{s}y = -my \tag{2.6}$$

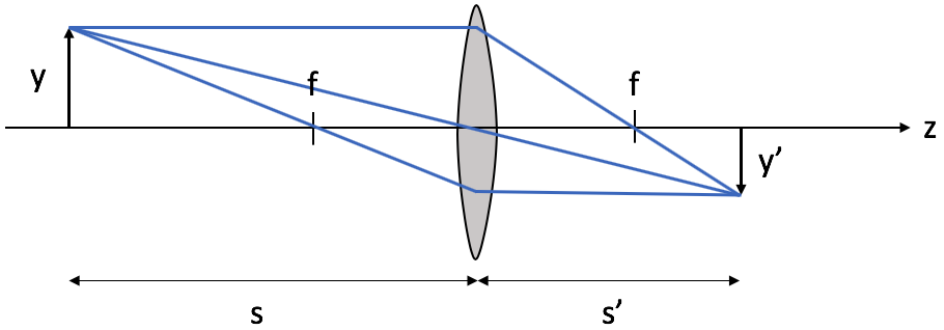

Figure 2.7: Example of an imaging system with a convex lens [21].

With the paraxial approximation, one can show that all rays originating from the object plane are focused at the image plane. This is unfortunately not the case in reality. Deviations from the ideal case are called aberrations. There are different kinds of aberrations which, in different ways, cause an imperfect image. Aberrations can be suppressed by having several lenses that compensates for these effects.

2.6.2 Afocal imaging system

An afocal system consists of at least two lenses. It is called afocal because it does not focus rays that are parallel to the optical axis like a normal lens does. A classical example is the Keplerian telescope [21], shown in Figure 2.8. It consists of two positive lenses with focal lengths: f_1 and f_2. Incoming parallel rays are focused by the first lens. If the second lens's focal point coincides with the first lens's focal point, the rays are imaged in infinity by the second lens. This system is also suitable for imaging with a specific magnification. A special case is if the object is placed at the focal point of the first lens. Then the image is at the focal point of the second lens. Such a system is shown in Figure 2.9. The magnification of this system is given by the ratio of the focal lengths of the two lenses: $M = f_1/f_2$. The magnification is the same no matter where the object is. The image plane is defined by the object plane and the magnification as: $z' = Mz$, where z' is the distance from the focal point of the second lens to the image plane, and z is the distance from the object plane the focal point of the first lens [21].

2.6.3 Throughput

The throughput of an optical system refers to how much power is captured from the object to form the image. There is a fundamental limit on the throughput of an optical system and is connected to a property of light called étendue. The étendue

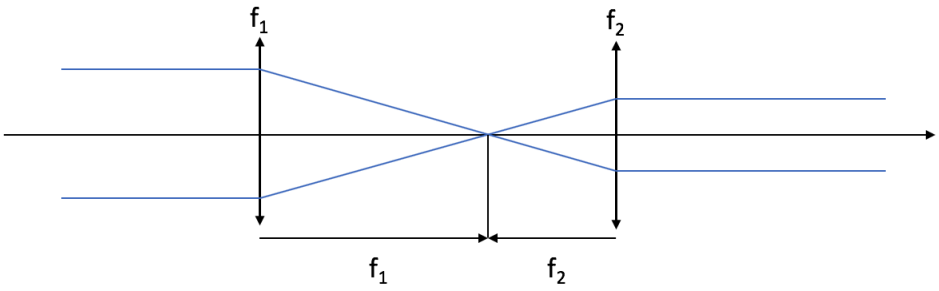

Figure 2.8: The Keplerian telescope [21].

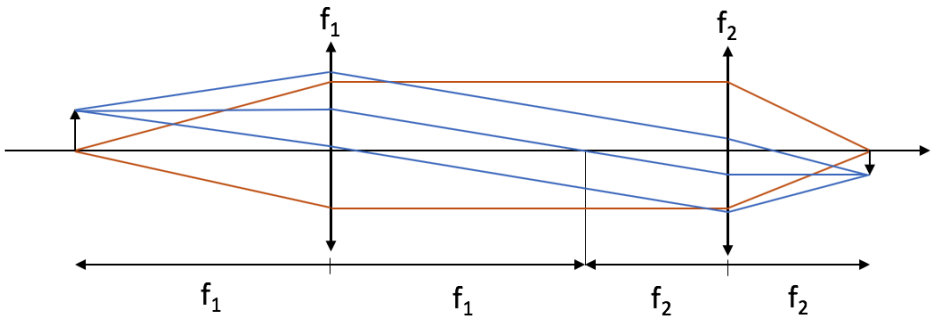

Figure 2.9: Imaging with an afocal system [21].

is an invariant through an optimal optical system [22]. In a real optical system, it changes, but it can never decrease. The étendue is defined by Equation (2.7), where S is the surface area that emits or receives light, and NA is the numerical aperture which defines the angular spread of the emitted or received light. It can be understood as a quantity describing how confined the light is. The concept is the same as the emittance of a particle beam.

Figure 2.10 shows a simple example of an optical system. A surface with an area S_e emits light with an angular extent θ_e, and numerical aperture, $NA = \sin\theta_e$. A lens is forming an image with an area S_r, which is defined by the magnification of the optical system. The light that the image receives has an angular extent θ_r, and the numerical aperture $NA = \sin\theta_r$. Since the étendue cannot decrease through the system, the étendue of the received light has to be larger or equal to the étendue of the emitted light [22].

$$G = \pi \cdot S \cdot NA^2 \tag{2.7}$$

When imaging into a fiber, the maximum receiving étendue is well defined. The fiber's numerical aperture is the maximum angular extent it can receive. Since the fiber has a maximum étendue that it can receive, and the étendue can never decrease, this is also the maximum étendue from the source that is transmitted through the system. If the source emits light with a larger étendue than the

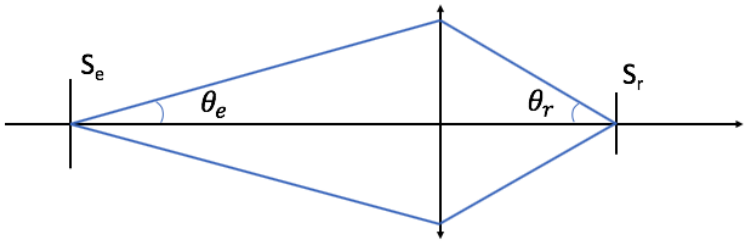

Figure 2.10: Illustration of étendue through an optical system. An emitting surface S_e is imaged by a lens to the receiving surface S_r.

possible receiving étendue, the fraction of the captured light can be calculated. This defines the maximal theoretical throughput.

An alternative estimation of the throughput can be done for a light source that has the same irradiance in all directions. The fraction of the light power captured by a lens is given by the solid angle of that lens. If the lens is placed at a distance, d, and has a diameter, D, the solid angle of the lens is given by:

$$\begin{aligned} \Omega &= 2\pi(1-\cos\theta) \\ \theta &= \arctan\big(\mathrm{D}/(2\mathrm{d})\big). \end{aligned} \tag{2.8}$$

Another way to express the amount of light the lens can capture is with the F-number. It is defined in Equation (2.9), where f is the focal length of the lens and D is the diameter. If $\mathrm{d} = \mathrm{f}$ and $\sin\theta \approx \theta$, the F-number can be expressed in terms of numerical aperture, $\mathrm{F} = 1/2\mathrm{NA}$, and the numerical aperture is connected to the solid angle.

$$\mathrm{F} = \frac{\mathrm{f}}{\mathrm{D}} \tag{2.9}$$

2.6.4 Resolution

In an imaging system, resolution is the ability to discriminate details in the object being imaged. The resolution can be defined and described in different ways. One way is how many line pairs per millimeter are resolvable [23]. A line pair is one white and one black line next to each other. The smallest size of a line pair that the imaging system can resolve defines the resolution of the imaging system. To resolve the line pair means that the two colors can be distinguished. Figure 2.11 shows three line pairs and the image from an arbitrary imaging system. The contrast in the line pairs is defined by the visibility, defined by Equation (2.10), where $\mathrm{I_{max}}$ is the maximum intensity (white line) and $\mathrm{I_{min}}$ is the minimum intensity (black line).

$$\mathrm{V} = \frac{\mathrm{I_{max}} - \mathrm{I_{min}}}{\mathrm{I_{max}} + \mathrm{I_{min}}} \tag{2.10}$$

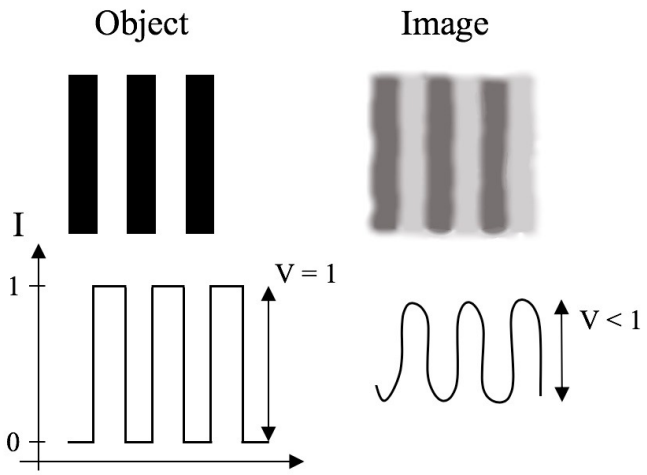

Figure 2.11: The visibility of line pairs after going through an imaging system. The left side of the figure shows the object and the normalized intensity, from left to right. The right side of the figure shows the image of the object and the normalized intensity. V is the visibility of the object end the image.

The visibility reduction through an imaging system as a function of spatial frequency (lp/mm) is called the Modulation Transfer Function (MTF) [23]. It is the system's response in the frequency domain. The inverse Fourier transform of the MTF is the Point Spread Function (PSF). This function describes the image of a point source. This is again connected to the resolution. The less the point is spread in the image, the smaller the details are that can be resolved by the imaging system.

Chapter 3
Characterization

In this chapter the characterization of the different parts of the system is presented. Every part have its own section where the method and the results are described. In all measurement the Experimental Physics and Industry Control System (EPICS) was used. This is a software environment that enables a client to control the Input Output Controller (IOC) of the devices used in the measurements. In the case of this thesis, MATLAB was used as the client. This was very convenient because both data acquisition and analysis could be done in the same script and could be run remotely.

3.1 Camera

3.1.1 Method

To characterize the camera, the EMVA Standard 1288 [18] is used. It is a standard for characterization of image sensors and cameras, that is commonly used in the industry. The method is to have a monochromatic, incoherent, homogeneous light source that illuminates the sensor, being characterized. A numerous images are collected at different light intensities. If also the power of the light can be measured, the responsivity and other properties of the camera can be calculated from this data. It is important that the light source is incoherent. A coherent light source would illuminate the sensor in-homogeneously due to speckles. Speckles are spatial variations of intensity due to constructive and destructive interference of the light.

A sketch of the setup used for this characterization is shown in Figure 3.1. To create a monochromatic, incoherent, homogeneous light source, a combination of components is used. First, is a incoherent, white light source from Thorlabs (MCWHF2) [24]. Right after the source, a diffuser and a green band-pass filter are placed. The diffuser makes the illumination on the sensor more homogeneous. The green band-pass filter, with a transmission at 532 nm, makes the light monochromatic. This filter is chosen because it is close to the wavelength of the light that the camera will detect in the final system. To measure the power of the light source, a beam splitter and a power meter are used. The transmitted light goes to the camera sensor and the reflected light goes to the power meter.

To know what the power is at the sensor, a preparatory measurement is done.

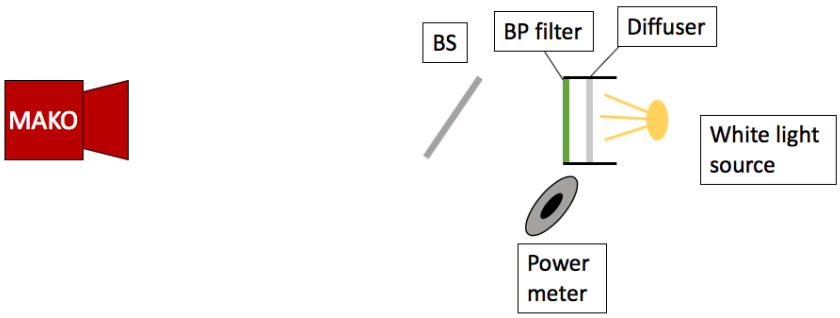

Figure 3.1: A sketch of the setup that was used for characterizing the camera.

First the power meter is placed right in front of the camera opening. The power is measured 20 times at 10 different light intensities. The power meter is then placed at the reflection of the beam splitter. The power is measured 20 times at the same 10 different light intensities. The power is also measured 20 times when the lights are off, so that the background could be subtracted. From this data, a linear relationship between the power at the reflection and the power at the camera sensor is found.

The power, P, can be converted into number of photons per pixel with the formula:

$$\mu_p = \frac{P \cdot t_{exp}}{E_{ph}} \frac{A_{pix}}{A_{pm}}, \tag{3.1}$$

where μ_p is the number of photons per pixel, t_{exp} is the exposure time, A_{pix} is the pixel area, and A_{pm} is the active area of the power meter. The energy of a photon is $E_{ph} = hc/\lambda$, where h is Planck's constant, c is the speed of light and λ is the wavelength of the light.

To follow the EMVA Standard, the signal can be varied in two different ways: either the incoming light intensity is varied, or the exposure time on the camera is varied. Both versions were done. First, the exposure time was varied. The mean power at the sensor was 653 nW. The diameter of the power meter was 9 mm. The exposure times were set to: 0.1, 9, 17.9, 26.7, 35.6, 44.5, 53.4, 62.2, 71.1, 80 [ms]. 20 images were collected at each exposure time. At every collected image, the power was measured. The same procedure was repeated with the light source off. For the second measurement, the exposure time was set to 20 ms. The intensity of the light source was set to 10 different values. This was varied by linearly changing the current to the LED. At each intensity, 20 images were collected. At each image, the power was measured. 20 images were also collected with the light source off, together with 20 measurements of the power.

The responsivity of the camera is calculated by taking the mean value of counts (digital value), minus the background, divided by the mean number of photons per pixel. See Equation (3.2). The noise of the camera is calculated for each set of 20 images. First, the standard deviation between the 20 images, for each pixel, is

calculated. This value is then squared, which gives the variance. The variance of the whole set of pixels is then calculated by summing up all the pixel variances and divide them by the number of pixels. The total standard deviation is then given by the square root of the total variance. See Equation (3.3), where x_n is the pixel value for image n, N is the total number of images (N = 20), μ is the mean number for every pixel, and image size is the total number of pixels per image.

$$\mu_y - \mu_{y.dark} = R\mu_p \tag{3.2}$$

$$\begin{aligned} \sigma_{pixel} &= \sqrt{\frac{1}{N}\big((x_1-\mu)^2 + (x_2-\mu)^2 + ... + (x_N-\mu)^2\big)} \\ \mu &= \frac{1}{N}(x_1 + x_2 + ... + x_N) \\ \sigma_{tot}^2 &= \frac{\sum \sigma_{pixel}^2}{\text{image size}} \end{aligned} \tag{3.3}$$

In the EMVA Standard 1288 [18], a relationship between the noise, system gain (K), and the mean number of counts is derived. See the result in Equation (3.4). This is called the photon transfer curve. When R and K are calculated, the quantum efficiency is easily found by: $\eta = R/K$.

$$\sigma_y^2 - \sigma_{y.dark}^2 = K(\mu_y - \mu_{y.dark}) \tag{3.4}$$

The smallest number of photons that can be detected is given by the dark noise divided by the responsivity:

$$\mu_{p.min} = \sigma_{y.dark}/R \tag{3.5}$$

and this varies with exposure time because the noise is varying with exposure time. The noise comes mainly from the dark electrons. A longer exposure time accumulates more dark electrons and contribute with a larger variance in the signal. In addition, there are still some photons in the room. These photons are collected during the exposure time and the amount increases with longer exposure times.

3.1.2 Results and Analysis

The results are presented in two different subsections: one for the measurement where the exposure time is varied, and one for the measurement where the intensity is varied.

Varying exposure time

The exposure time is set to 10 different values. At each exposure time, 20 images are taken. Every image has 1936 x 1216 pixels. The collection of data is done both with the light source on and the light source off. The total dimension of the data is therefore: 2 x 10 x 20 x (1936 x 1216). Additionally, the power is probed every time an image is collected.

The mean number of counts for each exposure time is calculated by taking the mean value for each image and then taking the mean value of the 20 images. This value is called μ_y. To calculate the standard deviation, σ_y, for each exposure time, Equation (3.3) is used. The mean number of counts, with the standard deviation as error bars, is shown in Figure 3.2a. It shows that the mean number of counts increases linearly with exposure time up to at least 60 ms. After that, the response rate is reduced due to saturation. This can also be seen in the standard deviation, shown in Figure 3.2b. It is increasing up to 60 ms and then drops. If some pixels are saturated, they have the maximum value (4096) for all 20 images and the standard deviation for these pixels is therefore zero. This lowers the total standard deviation of the data set.

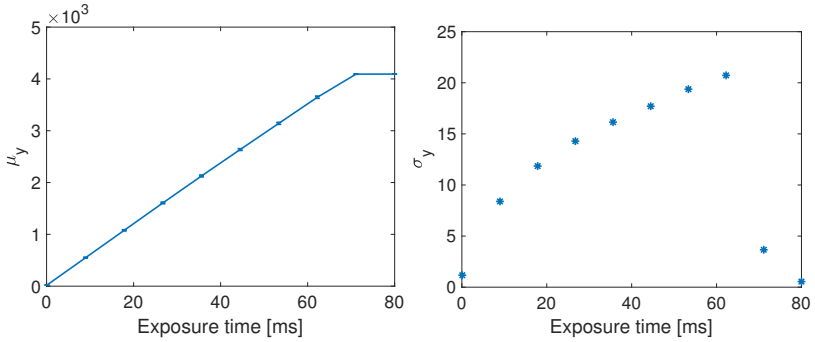

(a) Mean number of counts **(b)** Standard deviation

Figure 3.2: These figures show the mean number of counts and the standard deviation for 20 images for 10 exposure times.

In the dark measurement, the same calculations were done. The mean number of counts, $\mu_{y.dark}$, and the standard deviations of the dark measurement, $\sigma_{y.dark}$, are shown in Figure 3.3. They both increase with exposure time.

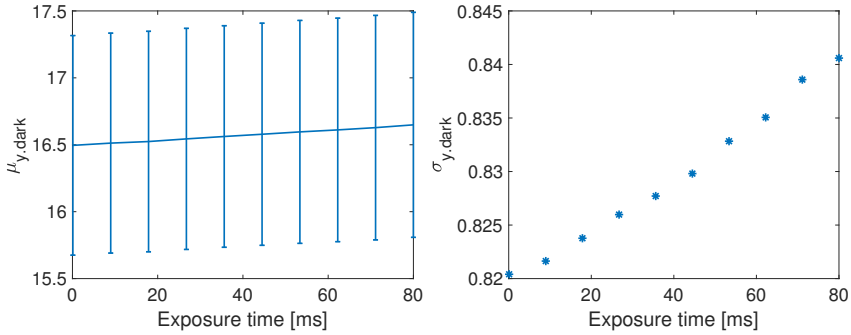

(a) Mean number of dark counts **(b)** Standard deviation for dark signal

Figure 3.3: These figures show the mean number of counts and the standard deviation for 20 dark images for 10 exposure times.

The signal to noise ratio (SNR) as a function of the mean number of photons is shown in Figure 3.4. Only the first 8 data points are shown since the 2 last points were taken when the sensor was saturated. The SNR is calculated with Equation (2.4). The mean number of photons is calculated with Equation (3.1). The power, P, is the mean power when the LED is on, minus the mean power when the LED is off. This value is then multiplied by the proportionality factor between the power at the reflection of the beam splitter and the power right in front of the camera. This factor is 2.2.

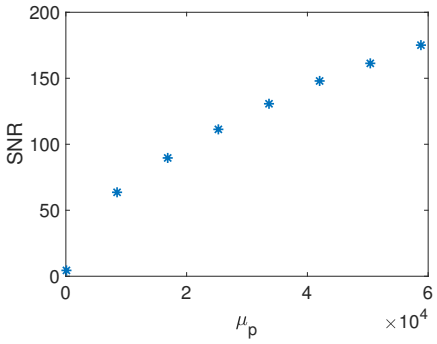

Figure 3.4: Signal to noise ratio as a function of mean number of photons.

The responsivity of the camera is calculated as the linear growth rate of counts as a function of incoming photons. The curve is shown in Figure 3.5a. A linear fit is done for the 8 first data points and the result is R = 0.0618. From the photon transfer curve (Equation (3.4)) the system gain is also found with a linear fit. The curve is shown in Figure 3.5b. It is done with the same first 8 data points. The result is K = 0.117. The quantum efficiency is then given by $\eta = R/K = 0.0618/0.117 = 0.5272$.

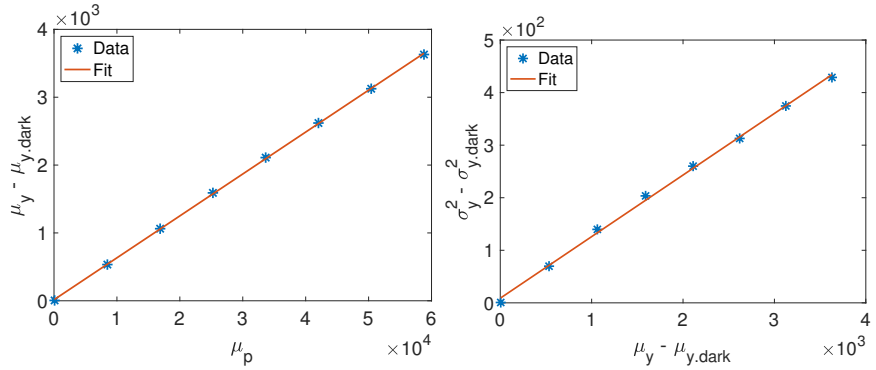

(a) Responsivity **(b)** Photon transfer curve

Figure 3.5: These figures show the responsivity and the photon transfer function.

Varying intensity

The intensity of the white light source is set to 10 different values. Every collection of data for a certain intensity is referred to as a data set. Each data set contains 20 images, and every image contains 1936 x 1216 pixels. The mean number of counts for each data set is calculated by taking the mean value of all pixel values for each image, and then taking the mean value of the 20 images. This value is called μ_y. The same is done for the images without illumination. This value is called $\mu_{y.dark}$. In Figure 3.6a, $\mu_y - \mu_{y.dark}$ is plotted for each data set, where the dark signal is $\mu_{y.dark} = 16.55$. The error bars are the standard deviation for each data set. This is calculated according to Equation (3.3). This is also plotted in Figure 3.6b. The dark noise is calculated to $\sigma_{y.dark} = 0.826$.

The number of counts is increasing with intensity but not linearly. The reason for this is the light source. The intensity is varied by changing the current in the LED, linearly. But the intensity is not linearly dependent on the current. However, this does not matter when the responsivity is calculated. See further down.

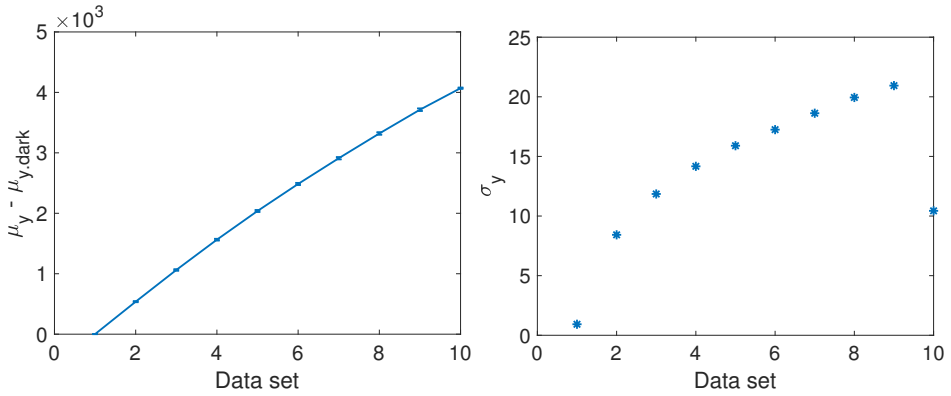

(a) Mean number of counts **(b)** Standard deviation

Figure 3.6: These figures show the mean number of counts and the standard deviation for 20 images for 10 different light intensities.

The number of incoming photons is again calculated with Equation (3.1). The power is measured for each intensity and multiplied by the proportionality factor which is measured to 2.0974 for this setup. Figure 3.7a shows the mean number of photons per pixel for each data set, with an error bar corresponding to the standard deviation.

The signal to noise ratio, plotted in Figure 3.7b, is calculated with Equation (2.4). The last data point is removed because the sensor was saturated. This is clear by looking at the standard deviation in Figure 3.6b. The last data point goes down abruptly, which happens when the sensor starts to saturate.

From this data, the responsivity and the system gain of the camera can be calculated. The responsivity is found by doing a linear fit of the mean number of counts as a function of mean number of photons. The fit is done for the first 8 data points. The last data points are not used because the camera was close to

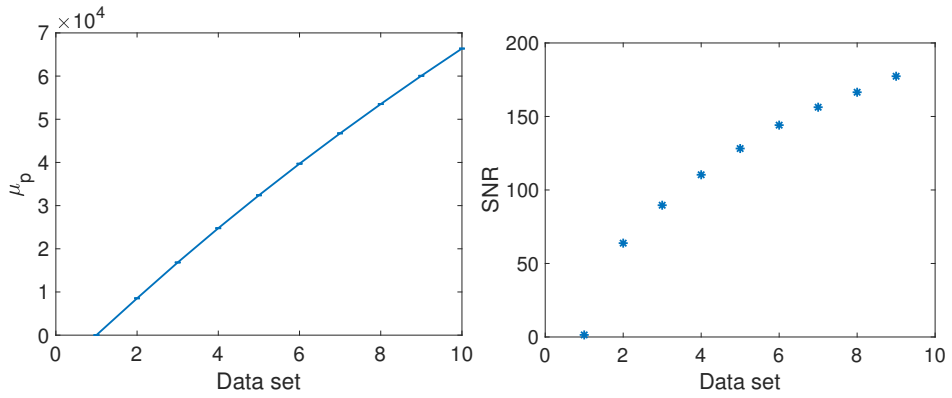

(a) Mean number of photons per pixel **(b)** SNR per pixel

Figure 3.7: These figures show the mean number of photons per pixel for 10 different light intensities and the signal to noise ration for the same 10 light intensities.

saturation for these points. The result from the fit is R = 0.0621. The system gain is found by doing a linear fit of the photon transfer curve. This is again done with the first 8 data points. The result is K = 0.118. The quantum efficiency at 532 nm is therefore $\eta = R/K = 0.0621/0.118 = 0.5278$.

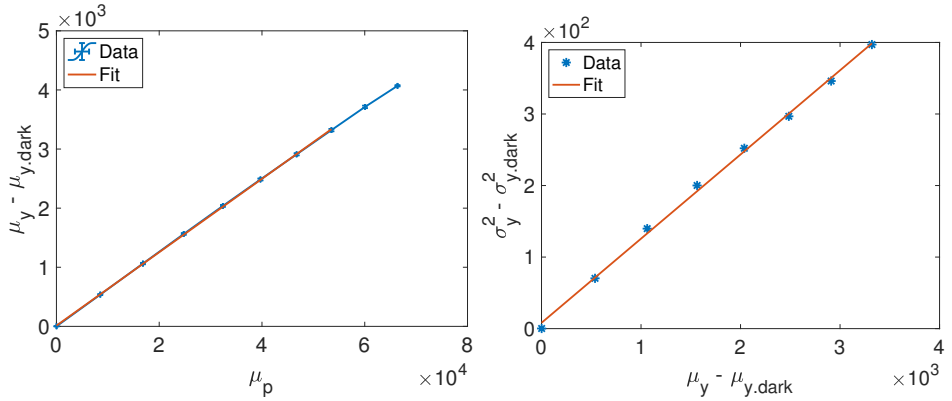

(a) Responsivity **(b)** Photon transfer curve

Figure 3.8: These figures show the responsivity and the photon transfer function.

Conclusions

A summary of the results is presented in Table 3.1. The table shows consistency between the two measurements. The responsivity, system gain and quantum efficiency differ by less than 1 %. For later calculations in the project, a responsivity of

0.062 is used. The minimum number of photons that can be detected can be estimated from the dark noise. When the signal is larger than the noise it is considered detectable. The minimum number of photons is therefore $\mu_{p.min} = \sigma_{y.dark}/R$.

Table 3.1: A summary of the results from the camera characterization

	Varying exposure time	Varying intensity
Responsivity	0.0618	0.0621
System gain	0.117	0.118
Quantum efficiency	0.5272	0.5278
Power at sensor	653 nW	0.717 nW - 2296 nW
Exposure time	0.1 ms - 80 ms	20 ms
Dark mean	16.5 - 16.65	16.55
Dark noise	0.82 - 0.84	0.826
Min. detectable photons	13.2 - 13.6	13.3

Figure 3.7 also gives a hint of the minimum detectable number of photons. The data point for the lowest intensity is SNR = 1.4. That corresponds to the first data point in Figure 3.7a which is 20 photons per pixel.

In both measurements, with varying exposure time and varying light intensity, the SNR has a square-root shape. This comes from the photon shot noise that is proportional to the square root of the number of photons. This is the dominant contribution to the noise for higher photon fluxes. For lower intensities, the standard deviation has some offset. The offset comes from the read-out noise. The increase with exposure time comes from the noise from the dark electrons, that increases linearly. The higher the light intensity is (or the longer exposure time) the more dominant the photon shot noise is.

3.2 Fiber

Before the fiber could be characterized it had to be assembled and connectorized. The fiber was thread through the outer protection called a furcation tube. Then the connectors at both ends were mounted and polished. This was done by hand with special tools from Thorlabs.

The fiber has two main features that were characterized: the transport of light intensity and the spatial resolution. It is important to characterize the loss of light intensity throughout the fiber because that has to be compensated for by the gain in the image intensifier. The resolution of the image is not only determined by the fiber structure, but also by the optics in front and in back of the fiber. The resolution is therefore characterized together with the optics.

3.2.1 Numerical Aperture

The first property of the fiber that was characterized was the numerical aperture. It was estimated by coupling light into one end of the fiber and studying the output at the other end. The output connector was placed at a distance, d, from a white screen. At the screen, a disc of diameter, D, was illuminated by the fiber. The diameter was measure with a ruler. From the distance, d, and the diameter, D, the numerical aperture could be calculated:

$$\mathrm{NA} = \sin\left[\arctan\left(\frac{D}{2d}\right)\right] \approx 0.5. \tag{3.6}$$

This matched the numerical aperture stated in the data sheet of the fiber.

3.2.2 Attenuation and Coupling

Method

The attenuation and coupling losses are described in Equation (2.3). To measure α and C, two fibers of different lengths were used. The first fiber, called Fiber 1, was 0.225 m long. The second fiber, called Fiber 2, was 8.5 m long. Fiber 2 is used in the complete system later. The coupling loss and the attenuation can be found by measuring the input power and the output power of the two different fibers. It was not trivial to measure the input power. Power is preferably measured with a power meter, but the fibers has a smaller input area than the power meter. Power meters integrate the irradiance over its area. If the input power to the fiber is calculated as the power on the power meter times the scaling factor, it is not correct. The transverse profile of the power may not be uniform and should be known. Figure 3.9 illustrates an example of the difference in power that a fiber and power meter can receive, due to their difference in size.

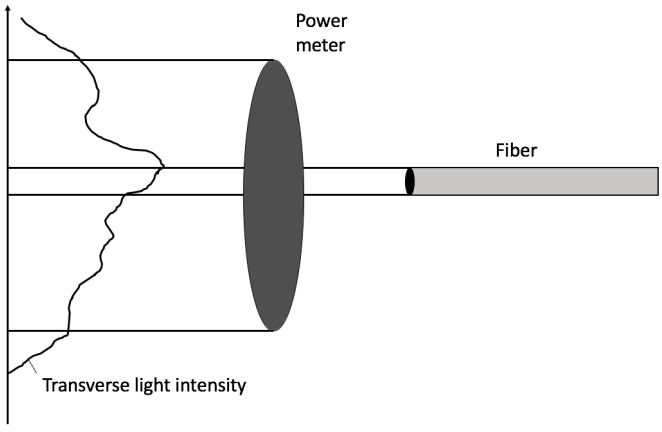

Figure 3.9: Sketch illustrating the difference in light intensity that the power meter and the fiber receives due to their different sizes, if the transverse light intensity is not uniform.

To account for this, the transverse intensity profile was made as uniform as possible. The same light source as in the camera characterization was used, which is the white LED followed by a diffuser and a band-pass filter. The input power was measured both with the power meter and the camera. The image on the camera can then be used to evaluate the flatness of the intensity. The output power was measured only with the power meter. The power meter was placed close to the output so that all intensity was captured by the power meter.

Two hundred images were taken with the camera, at the position where the fibers were placed later. One hundred of those images were taken with the light on, and one hundred with the light off, so that the background could be subtracted. Then, the same was done with the power meter. Fiber 1, was then placed at the input position and the power meter was attached to the output of the fiber. The power was probed one hundred times. Then the connectors of the fiber were switched and the measurement was repeated. The same thing was done for Fiber 2.

Results

The power per square meter, irradiance, was measured both by the camera and the power meter. These results are shown in Table 3.2. The irradiance measured by the camera was calculated by this formula:

$$\mathrm{I} = \frac{\mu(\mathrm{counts})}{\mathrm{R}} \cdot \frac{\mathrm{E_{ph}}}{\mathrm{A_{pixel}} \cdot \mathrm{t_{exp}}}, \tag{3.7}$$

where μ(counts) is mean number of counts per pixel for all 100 images, R is the responsivity of the camera (0.062), $\mathrm{E_{ph}}$ is the energy of one photon, $\mathrm{A_{pixel}}$ is the area of a pixel ($3.434 \cdot 10^{-11}\mathrm{m}^2$) and $\mathrm{t_{exp}}$ is the exposure time (5 ms).

Table 3.2: Input irradiance, measured with the camera and the power meter (PM).

Irradiance camera	Irradiance PM
$0.0147\,\mathrm{W/m^2}$	$0.0143\,\mathrm{W/m^2}$

The input power, $\mathrm{P_{in}}$, was then calculated by multiplying the input irradiance by the input area of the fiber. The area is $(0.0015/2)^2 \cdot \pi = 1.7671\,\mathrm{mm}^2$.

The results of the output power, $\mathrm{P_{out}}$, calculated coupling loss and attenuation loss are shown in Table 3.3. The attenuation coefficient, α, is calculated by combining the results from the two fibers into Equation (2.3), as shown in this formula:

$$\alpha = \frac{\ln(\mathrm{P_{out,1}}/\mathrm{P_{out,2}})}{\mathrm{L_2} - \mathrm{L_1}} = 0.0905\,\mathrm{m^{-1}} = 0.393\,\mathrm{dB/m}, \tag{3.8}$$

where $\mathrm{P_{out,1,2}}$ is the mean value of the two results in Table 3.3, and $\mathrm{L_{1,2}}$ were the lengths of the fibers. When α is found, the coupling loss can be calculated with Equation (2.3). $\mathrm{P_{in}}$ is the mean value of the two numbers shown in Table 3.2.

Table 3.3: Fiber output power, and coupling and attenuation losses. (12) and (21) refers to the order of the connectors.

Fiber	Power out (nW)	Coupling loss	Attenuation loss
Fiber 1 (12)	14.878	0.5929	0.9798
Fiber 1 (21)	14.768	0.5886	
Fiber 2 (12)	7.0144	0.5911	0.4634
Fiber 2 (21)	7.0056	0.5904	

To evaluate the flatness of the transverse light intensity, the images taken by the camera are analyzed. First, the mean value of the 100 images is calculated. The mean value over the two separate dimensions is calculated, and plotted in Figure 4.3. The plots show that the intensity has a gradient over the sensor. However, the difference between the maximum and the minimum pixel value is 2.6 %. This is considered to be small enough to approximate it as a constant transverse irradiance.

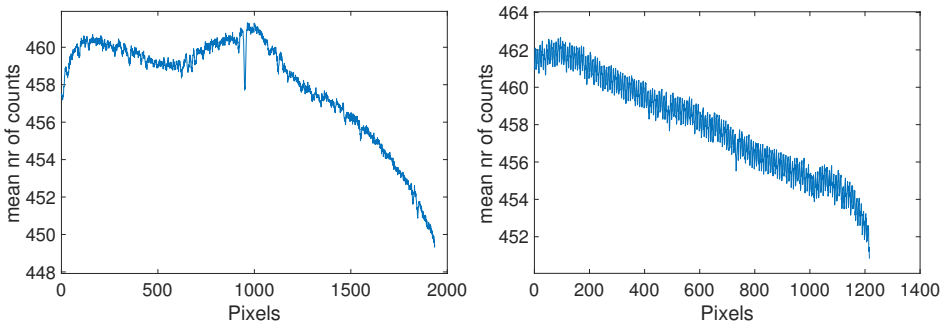

(a) Mean number of counts along the y-axis.

(b) Mean number of counts along the x-axis.

Figure 3.10: These figures show the mean number of counts along the x and y direction over the camera sensor, when being illuminated.

3.2.3 Core size

A fundamental limit of the resolution of an imaging fiber is the size of the cores. Therefore, a measurement to find the size of the cores was done. One end of the fiber was illuminated with a white light source. The other end was imaged onto the camera sensor. The imaging lens system consisted of two plano-convex lenses with focal lengths 100 mm and 35 mm. The fiber output was placed at the focal length of the 35 mm lens. The camera sensor was placed at the focal length of the 100 mm lens. This system has a magnification of 2.86. The cores of the fiber is visible in the image of the camera. The size of the cores can therefore be calculated by counting the pixels in the image. A more accurate measurement

was done. The core size was calculated by performing a spatial discrete Fourier transform of the image. The Fourier transform reveals the spatial frequency of the fiber. This is directly connected to the period of the core pattern and therefore the distance between the cores. The image of the fiber connector and its Fourier transform are shown in Figure 3.11. The Fourier transform was performed with the two dimensional fast Fourier transform function, fft2, in MATLAB.

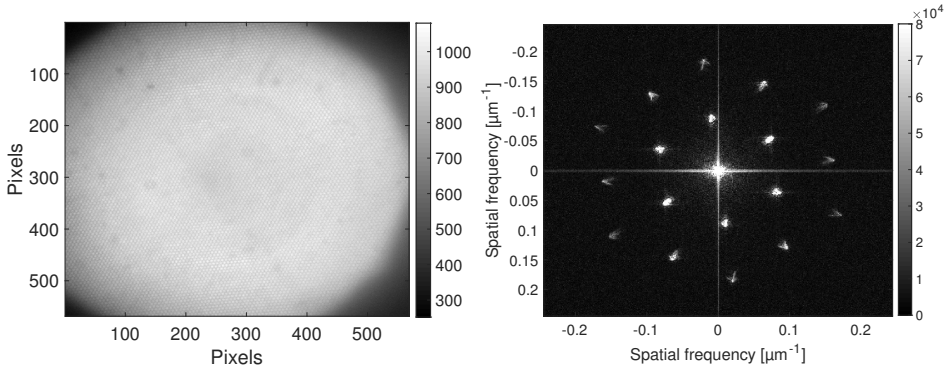

(a) Image of the fiber connector **(b)** Fourier transform of the image in a)

Figure 3.11: These figures show the image of the fiber bundle input and the Fourier transform of the image.

The bright spot in the middle of the Fourier transform is the zeroth frequency. The six bright spots forming a circle around the center come from the pattern of the cores. The upper half of the image contains the same information as the lower half because the Fourier transform always gives a negative copy of all the frequency components. The three upper dots corresponds to three directions in the pattern with an dominant frequency.

To find the period of the core pattern, the frequency axis from the Fourier transform had to be calculated first. The discrete frequency axis is given by:

$$f = \frac{\mathrm{M}}{\text{Pixel size}} \cdot (-0.5 : 0.5), \tag{3.9}$$

with the same length as the image size (568 pixels). The period of the pattern is then calculated by taking the average distance between the three upper spots to the zeroth frequency. The inverse of the average spatial frequency gives the spatial distance, 10.85 µm. This corresponds to 46 lp/mm if one line pair covers two cores.

3.2.4 Imaging Resolution Through Fiber

Method

To characterize the resolution of the image through the fiber, the Modulation Transfer Function (MTF) was searched. A common way to measure the MTF is to use the 1951 USAF resolution test chart. It is a resolution test pattern developed by the U.S. Air Force MIL-STD-150A standard of 1951. It consists of

line pairs of different sizes. By imaging this target, the visibility of each line pair frequency can be found, which defines the MTF of the system.

Three different imaging systems were tested. System 1 consists of a camera lens from the company Navitar. It has a focal length of 35 mm. The F-number ranges from 1.4 to 16 and 1.4 was chosen in this setup to maximize the light intensity. The second system is a bi-convex single lens. It has a focal length of 35 mm and is one inch in diameter. That corresponds to a F-number of 1.45. The third system consists of two plano-convex lenses, which form an afocal imaging system. The two lenses have the focal lengths: $f_1 = 35\,\text{mm}$ and $f_2 = 150\,\text{mm}$. Both lenses have a diameter of 1 inch. The magnification of this system is given by the ratio of the focal lengths: $M = 35/150 = 0.23$.

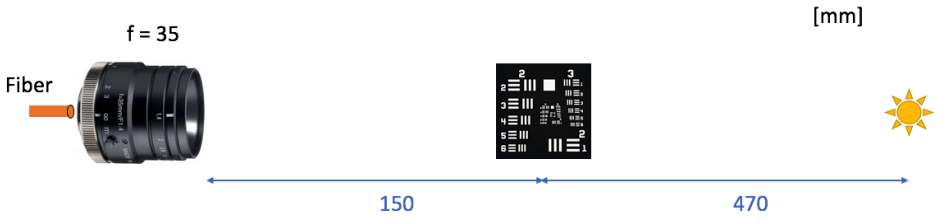

(a) Imaging system 1

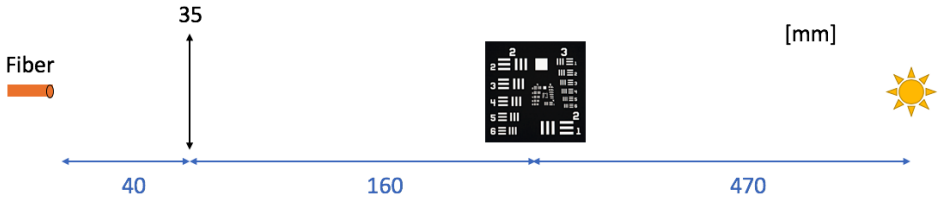

(b) Imaging system 2

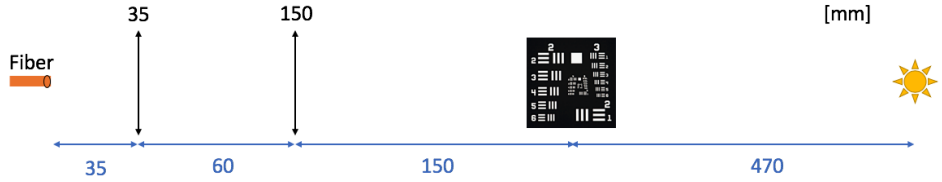

(c) Imaging system 3

Figure 3.12: The three imaging systems tested for imaging resolution through the fiber. The sun represents a white light source.

To be able to compare the three systems, the magnification should be the same. In system 1 and 2, the object was therefore placed to get as close to $M = 0.23$ as possible. The object that was imaged was a USAF target from Thorlabs (R1DS1N). It has a frequency from 4 lp/mm to 228 lp/mm. Behind the object, a white light source was placed. Figure 3.12 shows the setups of the three systems. The distances in the figure were measured with a ruler. On the other side of the fiber, a second imaging system was placed to detect the image with the MAKO G-234 camera. This system consists of two lenses with focal lengths:

$f_1 = 25.4\,\text{mm}$ and $f_2 = 100\,\text{mm}$.

One image was acquired for each system. To be able to compare the images, the light source had the same intensity for all images and the exposure time on the camera was the same, 0.488 ms. The measurement was also done two days in a row. All systems were unmounted and mounted again the next day. This was done to see how sensitive the measurement was to alignment differences. Therefore, 6 images were taken in total. For each image, the MTF was calculated.

The 1951 USAF target is divided into groups. Each group has 6 elements. For every element, there are three vertical and three horizontal line pairs. To calculate the visibility of one element, the region of that element in the image is selected. The mean value along the direction of lines is calculated. In case there is a gradient background illumination, this is subtracted. The peaks and the valleys of the mean-value-curves are identified. Then the mean value of these peaks and valleys are calculated. These values are put into Equation (2.10) as I_{max} for the mean-value-peaks and I_{min} for the mean-value-valleys, to calculate the visibility, V. This is done for all the elements in the image, where peaks and valleys can be identified. Every element has a spatial frequency which is calculated by dividing the target's frequency by the magnification of the imaging system.

Results and Analysis

The magnification of the three systems on the two different days are presented in Table 3.4. It was not trivial to align for a specific magnification. Therefore the magnification for system 3 differs a bit from the other two. Since the magnification was included in the calculations of the MTF, it did not effect the final result.

Table 3.4: The measured magnification for the three imaging systems for the two days of measurements.

	Day 1	Day 2
System 1	0.252	0.252
System 2	0.2813	0.3008
System 3	0.252	0.2505

The six images are shown in Figure 3.13 and all MTFs are plotted in Figure 3.14. Notice that the scale of the images is an inverse gray scale. This means that black represents a higher intensity than white. During the measurement, it was very difficult to get an image with uniform illumination and resolution. All of the images have a varying resolution throughout the image. This is also visible in the MTF plot. The MTF usually decreases with frequency. The plot shows that all six functions have a dip at approximately 20 lp/mm, that is followed by a local peak. These can be explained from the position of the elements in the target. For example, in Figure 3.13, Day 1, System 1, one can see that group 2 is on the right side of the image. This part has a lower resolution than the left side. Group 3 is in the left part of the image. When the MTF functions comes to the first element in the third group, the resolution therefore goes up.

None of the systems have a significantly better resolution than the others. However, there are some practical differences between them. System 2 is the most simple system. Compared to system 3, it requires less space to achieve the same magnification. System 3, on the other hand, is easier to align for a specific magnification. System 1 has the most expensive lens, but would be easy to align with the adjustable focus. System 1 should theoretically be the best because it contains optics that compensates for stray light and aberrations. These measurements were probably not sensitive enough to detect such a difference.

In system 3, the distance between the lenses is, for practical reasons, shorter than the distance described in Chapter 2. However, if the object and the image are placed in the focal points of the two lenses, the rays between the lenses are parallel to the optical axis. It is therefore not critical that the two focal points coincide between the lenses. This was also confirmed in a separate measurement.

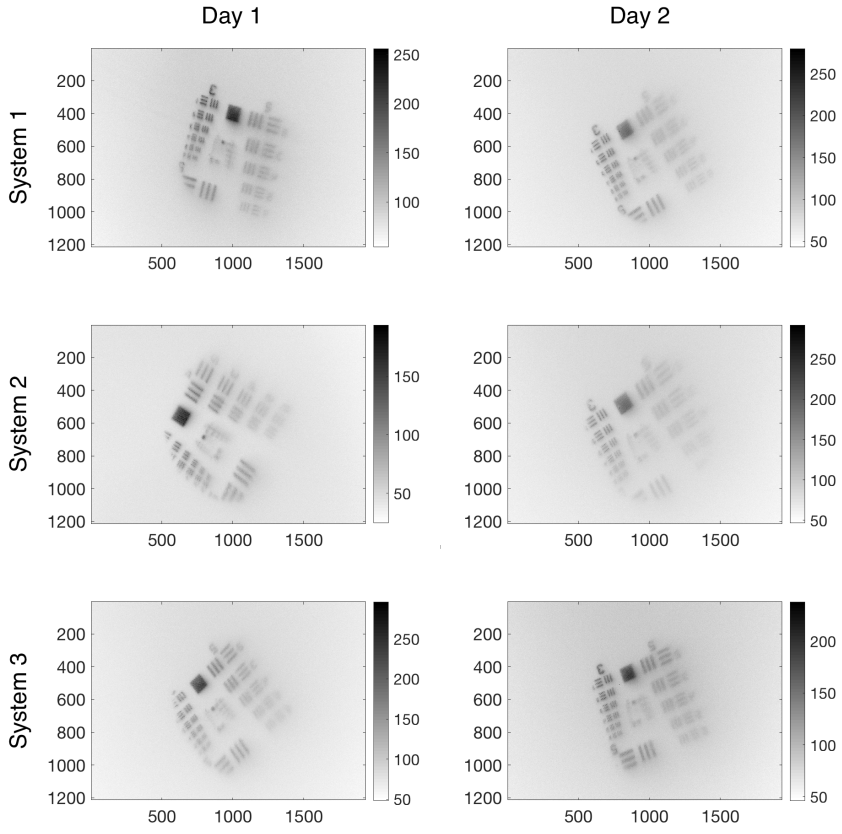

Figure 3.13: Images taken for calculating the MTF of three different imaging systems. The same measurements were done on two different days. The images have an inverse gray scale.

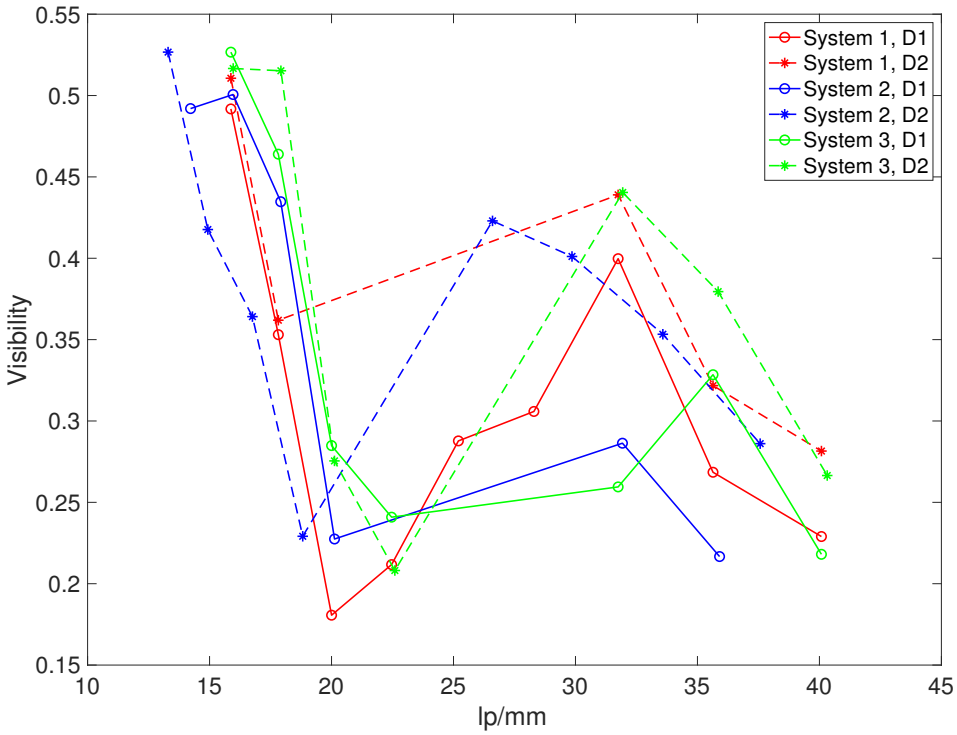

Figure 3.14: Visibility as a function of spatial frequency, calculated for the images in Figure 3.13. D1 and D2 refer to day 1 and 2.

Throughput

The throughput of the three imaging systems can be estimated with the solid angle that the lens covers from the distance of the object. All three systems have the same lens diameter: 1" = 25.4 mm. They also have approximately the same distance from the object, 150 mm. The solid angle is:

$$\Omega = 2\pi\left(1 - \cos\left[\arctan\frac{25.4}{2 \cdot 150}\right]\right) = 0.0224. \tag{3.10}$$

This number can be compared with the theoretical limit, defined by the étendue. The fiber has an input surface area of $A_f = \pi \cdot 0.75^2 = 1.77\,\text{mm}^2$. The fiber also has a numerical aperture of 0.5. The étendue that the fiber is capable of receiving is given by Equation (2.7), and is calculated as follows:

$$G_r = \pi \cdot A_f \cdot NA^2 = \pi \cdot 1.77 \cdot 10^{-6} 0.5^2 = 1.3879 \cdot 10^{-6}. \tag{3.11}$$

Since the étendue never decreases, the maximum emitted étendue can be derived

by setting it equal to G_r:

$$\begin{aligned} G_e &= G_r = 1.3879 \cdot 10^{-6} \\ G_e &= \pi \cdot A_e \cdot \sin^2 \theta \\ \theta &= \arcsin \sqrt{\frac{G_e}{\pi \cdot A_e}} \\ \Omega &= 2\pi(1 - \cos\theta) = 0.0437, \end{aligned} \tag{3.12}$$

where A_e is the area of the output surface of the image intensifier ($32\,\mathrm{mm}^2$), which becomes the emitting surface in the final system. The estimated throughput of the three system was about 50 % of what could theoretically be transmitted. One reason for not reaching a higher throughput is that the light propagating from the lens to the fiber was more confined than the fiber could receive. The numerical aperture is about 0.35, though it could be as high as 0.5. To increase the throughput, a lens with a NA = 0.5 should be used. That is equal to an F-number of 1.

By analyzing the formula for the étendue, the theoretical throughput as a function of emitting area, A_e, can be found. If the throughput, or transmission, is defined as $T = \Omega/2\pi$, it describes how much of the emitted light is captured by the lens. This is plotted as a function of A_e in Figure 3.15. The plot shows clearly that a smaller Fiber Optical Plate would potentially give a larger throughput.

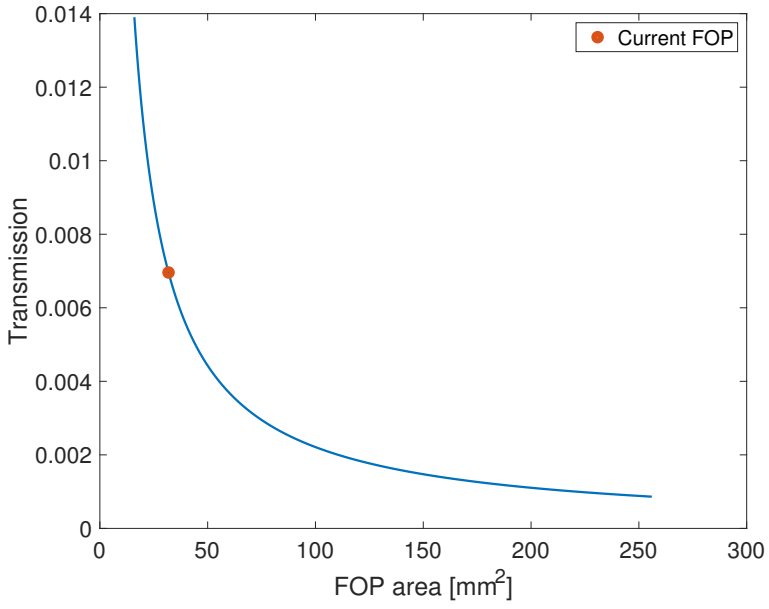

Figure 3.15: Transmission through lens 2 as a function of Fiber Optical Plate (FOP) area.

3.3 Image Intensifier

3.3.1 Method

In this measurement, the responsivity of the Image Intensifier (II) was searched. The gain in the MCP could be varied by varying the voltage over the MCP. The responsivity was measured for three different MCP-voltages: 600V, 800V and 1kV. The responsivity in this case was understood as how many photons were coming out from the II as a function of the total number of photons coming in. To find that, the input power was measured with the power meter and the output power was measured with the MAKO G-234 camera, while the light intensity was varied.

A similar light source-setup as in the camera characterization was used. Figure 3.16 shows a sketch of the experimental setup. First, the white LED from Thorlabs is placed. In front of the light source are a density filter and a low-pass filter. The low-pass filter transmitts all wavelengths longer than 605 nm. In the analysis, 608 nm is used as the peak wavelength of the incoming light. Between the light source and the II, a beam splitter is placed. The transmitted light goes to the II and the reflected light goes to the power meter. This enables the input power to be measured simultaneously as the output power. A preparatory measurement was done to find the linear relationship between the power at the reflection of the BS and right in front of the image intensifier. This is the same measurement as in the camera characterization. For more details about this preparatory measurement, read section 3.1.1. The linear factor between the two positions of the power meter, is 4.8608.

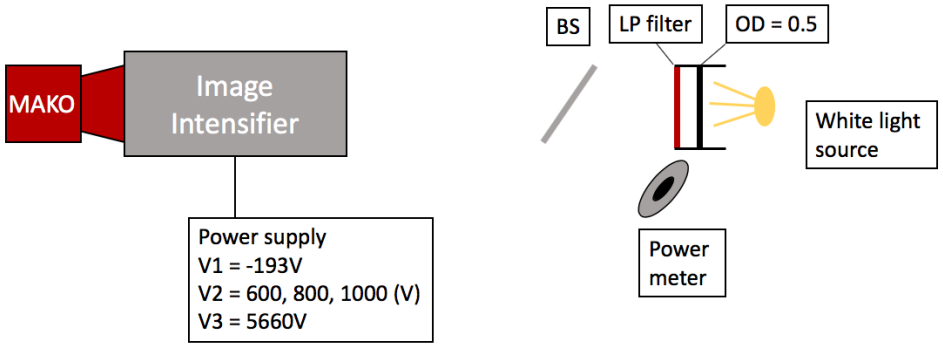

Figure 3.16: Experimental setup for characterizing the image intensifier.

The output power was measured with the camera mounted 34 mm behind the FOP surface. The total number of photons can be calculated with Equation (3.13), where sum(counts) is the summed up pixel values, background is the sum of the dark image, R, is the responsivity of the camera (0.062), t_{exp} is the exposure time (0.2 s), and Ω is the solid angle of the camera sensor. The camera sensor sits 15 mm from the opening. The size of the sensor is 10.67 x 8 mm. To calculate the solid angle, the sensor is approximated to be a circular surface with a radius of 5 mm. The total distance between the output of the II and the sensor is 49 mm. The

fiber taper at the back of the image intensifier has a numerical aperture of 1. The emitted light is therefore assumed to have the same irradiance in all directions. The light can be described as having a solid angle of $\Omega_{light} = 2\pi$. The fraction of light that is detected by the camera can be estimated by the fraction of the solid angle of the emitted light and the sensor: $\Omega/2\pi$.

$$\mathrm{ph_{out}} = \frac{\mathrm{sum(counts)} - \mathrm{background}}{\mathrm{R} \cdot \Omega/2\pi \cdot \mathrm{t_{exp}}} \tag{3.13}$$

The total number of incoming photons is calculated with the formula:

$$\mathrm{ph_{in}} = \mathrm{P} \cdot 4.8608 \cdot \frac{\mathrm{A_{II}}}{\mathrm{A_{pm}}} \frac{1}{E_{ph}}, \tag{3.14}$$

where P is the power, $\mathrm{A_{II}}$ is the area of the image intensifier input window, $\mathrm{A_{pm}}$ is the area of the power meter, and $\mathrm{E_{ph}}$ is the energy of the photons.

The light source was set to 9 different light intensities. At each intensity, 10 images were acquired and the power was probed before each image was acquired. The mean value for each set of 10 images was calculated. The same was done with the power. Ten images and powers were acquired with the light source turned off to measure the background signal. The background was then subtracted from the measured values. This was repeated for three different gain voltages.

3.3.2 Results and Analysis

In Figure 3.17a the number of photons coming out is plotted as a function of number of photons coming in, for the three voltages. For the lowest voltage (600 V), the response is linear. For 800 V the gain started to show saturation effects for higher input powers. The largest voltage is clearly saturated for the highest number of incoming photons. The slopes of the curves (before saturation) is the responsivity for each voltage.

To see the responsivity clearer, the same data is plotted in Figure 3.17b, but with a y-axis showing $\mathrm{R} = \mathrm{ph_{out}}/\mathrm{ph_{in}}$. The responsivity is fluctuating a bit for the low intensities. That can come from the uncertainty in the measurement of the power. The lowest number of photons is on the threshold of what the power meter can detect. Another thing that can be observed in Figure 3.17b, is that the gain does not increase linearly with the voltage. For 600 V, the responsivity is about 2, 800 V it is of about 30, and for 1 kV, it is up to 350. This is expected due to the nonlinear mechanisms in the MCP.

In the responsivity, the quantum efficiency of the photocathode is included. To find the gain of the MCP the responsivity has been divided by the quantum efficiency. The quantum efficiency for 608 nm is about 5 %. The highest gain for 1 kV is therefore 7000. This number is interesting because it gives the number of photons for each incoming photon that is absorbed. Because light is quantified in photons, the output signal will either be 0 or 7000 $\pm$ noise, and not something in between. The noise can therefore be ignored.

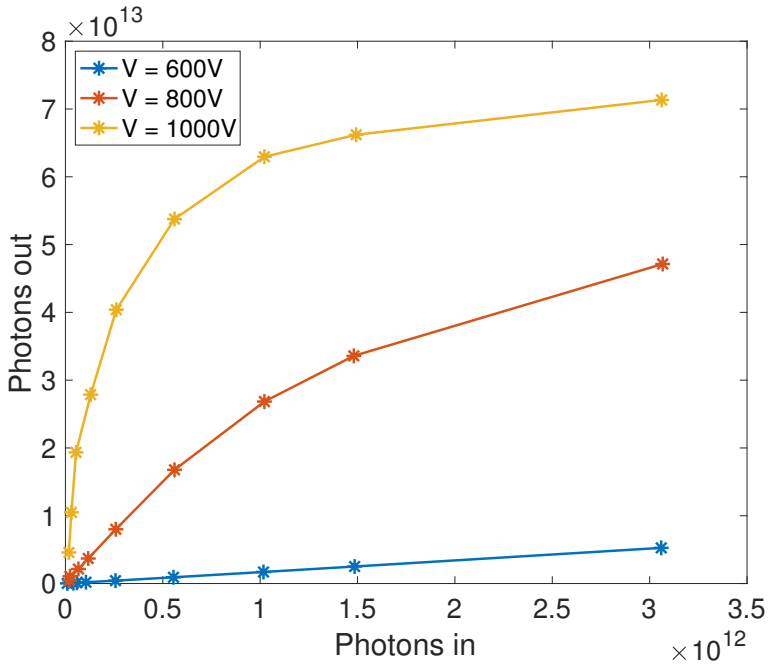

(a) Number of photons out as a function of photons in for three different voltages over the MCP.

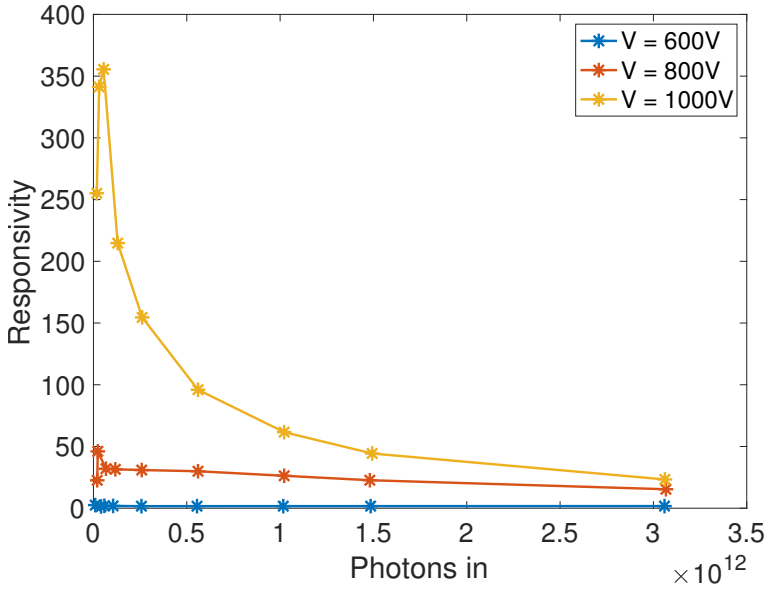

(b) Responsivity of the image intensifier for three different voltages over the MCP.

Figure 3.17: These figures show the responsivity of the image intensifier expressed in two different ways, for three different voltages over the MCP.

3.4 Single Photon Detection

3.4.1 Method

Unfortunately, the gain of the image intensifier was too low to detect single photons through the whole system. Despite this, one final measurement of the whole system was done to demonstrate the required gain for single photon detection. The experimental setups for this measurement are shown in Figure 3.18. A point source was generated by focusing a laser onto a white screen. To be able to vary the intensity of the light source, a filter wheel was placed in the beam path. The filter wheel has 6 neutral density filters. In front of the image intensifier, a 35 mm objective lens was placed, to image the point source onto the input window of the II. This was the same lens as in imaging system 1, in Figure 3.12a. The gain voltage on the image intensifier was set to 800 V. After the image intensifier, any of the three imaging systems, characterized earlier, could have been used. Imaging system 3 (Figure 3.12c) was chosen, because it was the easiest to align. To image the fiber onto the camera, the same optics as in the earlier measurements was used, for practical reasons. This last optical system was assumed to have negligible losses and assumed to not limit the overall resolution.

To find the required gain to detect single photons, the output image of the point source from the image intensifier (Setup 2, Figure 3.18b) was compared with the output image after the whole system (Setup 1, Figure 3.18a). First, images were acquired with setup 1, for a varying point source intensity. From this measurement, the smallest required intensity for detecting the point source, could be found. Images were then acquired with setup 2. A 50 mm lens was used to image the output to the camera. These images could then be used to calculate the required number of photons emitted by the image intensifier, that corresponded to the intensity where the point source could be detected in setup 1. This gave the required responsivity of the image intensifier for single photon detection.

At each filter on the filter wheel, 20 images were taken. The exposure time on the camera was 2 s for both setups. 20 images were also taken in the dark to measure the background. The mean value of the background was then subtracted from the other images. To count the number of emitted photons from the II, the image was fit to a 2D Gaussian. The volume of the Gaussian was calculated. This value was then divided by the responsivity of the camera (0.062). To get the total number of emitted photons, the value was also divided by the fraction of light that the lens captured. This was calculated with the formulas:

$$\begin{aligned} frac &= \frac{\Omega}{2\pi} = 1 - \cos\theta \\ \theta &= \arctan(25.4/2/95), \end{aligned} \tag{3.15}$$

where 95 mm is the distance from the II output to the lens and 25.4 mm is the diameter of the lens.

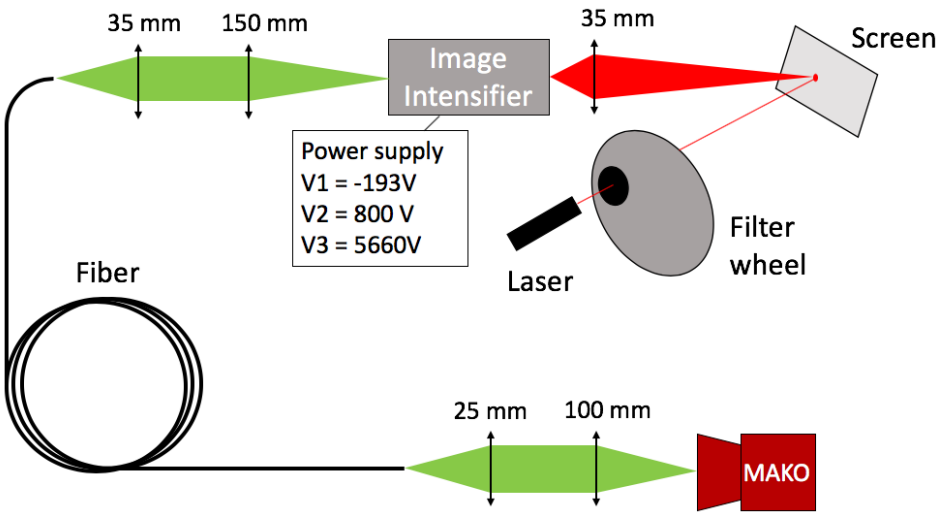

(a) Setup 1 for single photons detection measurement.

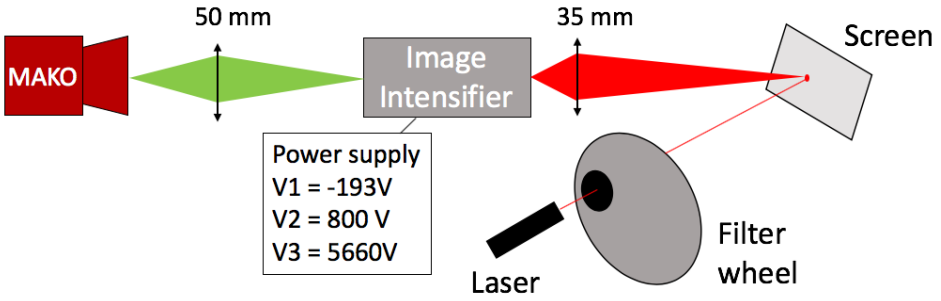

(b) Setup 2 for single photons detection measurement.

Figure 3.18: The experimental setups for demonstrating single photons detection requirements. Setup 1 contains the whole non-invasive profile monitor (NPM).

3.4.2 Results and Analysis

The images that were taken with setup 1 are shown in Figure 3.19. Even though 20 images were taken at each filter, only the 10th image at each filter are shown in the figure. A region of interest (200x200) was selected for all images. Furthermore, pixels with high intensity due to dust particles on the camera sensor were removed. This helped the fitting function to find the fit. The red ellipses represent the standard deviation from the Gaussian fit. The fit parameters are also presented in Table 3.5. The volume of the Gaussian function was calculated as: $V = 2\pi I_{peak}\sigma_a\sigma_b$. The fit seemed to work up to filter 5, but not for filter 6. These two intensities were further investigated by performing the fit to all 20 images for each filter. All 20 images from filter 5 could be fitted to the 2D Gaussian and non of the images from filter 6 could be fitted. From the 20 fits, a standard deviation of the calculated volume could be found. This was about 10% of the mean value. Filter number 5 was therefore considered to be the lowest intensity where the point source could be detected. The point source was considered to not be detectable with filter number 6. The threshold for detection therefore had to be somewhere between filter 5 and filter 6.

The images that were taken with setup 2 are shown in Figure 3.20. These images show the mean value for each pixel among the 20 images taken with each filter. A region of interest (130x130) was selected for all images. Every image was fitted with a 2D Gaussian function. The red ellipses represent the fit. The fit parameters, the calculated volume and emitted photons are summarized in Table 3.6. The number of photons was calculated as the volume divided by the responsivity of the camera and the fraction of light that the lens captured. In the images in Figure 3.19, it was concluded that the threshold goes between filter 5 and 6. This means that the required number of photons emitted from the image intensifier is somewhere between $0.42 \cdot 10^7$ and $3.02 \cdot 10^7$ photons. This is also the required gain.

The difference between the data and the fitted function indicates that the data is not really a Gaussian function. It resembles more a Lorentzian function. A Lorentzian function has longer tails going out from the peak, while the Gaussian has a more constant background. This means that the fitting parameters are not very accurate but still good enough to make estimations.

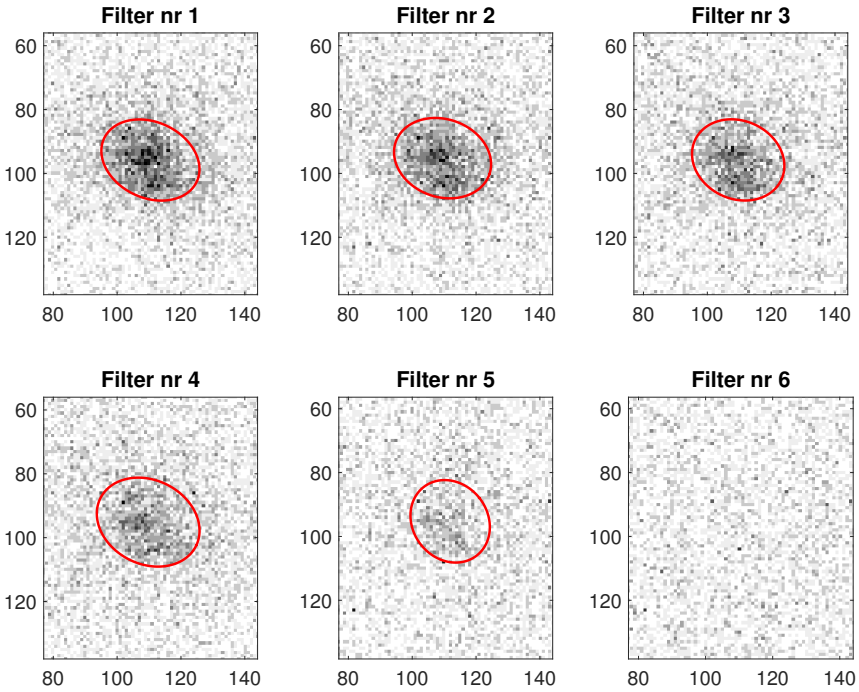

Figure 3.19: Images of a point source, taken with setup 1, for six different neutral density filters. The red ellipses are drawn with the parameters from the 2D Gaussian fits. All images have the same color scale and black means higher intensity than white.

Table 3.5: Parameters of the 2D Gaussian fit for the images taken with setup 1.

	Peak	σ_a	σ_b	Volume
Filter 1	3.44	16.0	11.9	4112.4
Filter 2	3.02	15.5	12.2	3586.0
Filter 3	2.57	14.5	12.2	2940.4
Filter 4	2.05	16.7	13.1	2828.7
Filter 5	1.27	11.7	13.6	1271.5

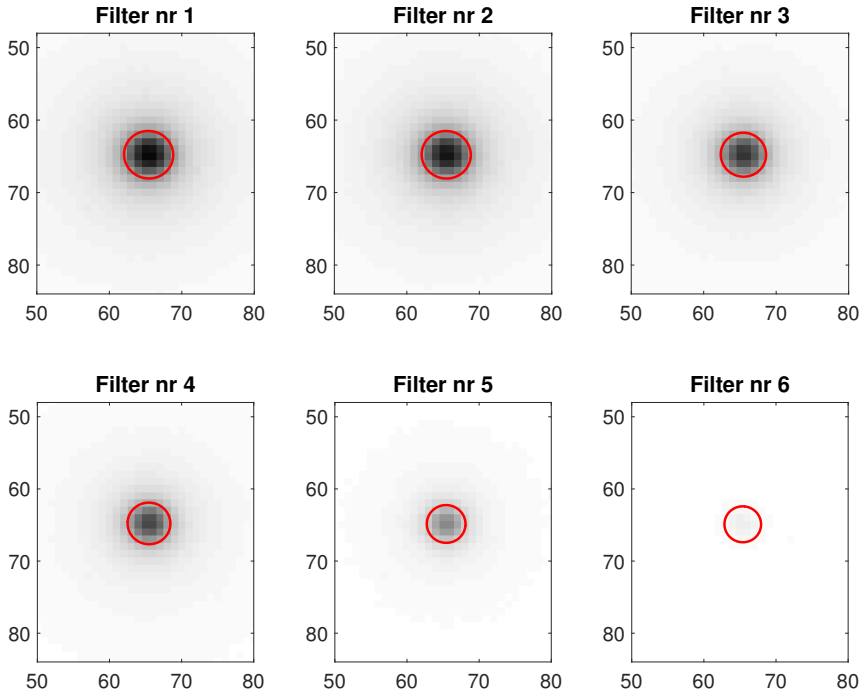

Figure 3.20: Images taken by the camera at the back of the image intensifier. The red ellipses represent the Gaussian fit. All images have the same color scale and black means higher intensity than white.

Table 3.6: Parameters of the 2D Gaussian fit for the images taken with setup 2.

	Peak	x_0	y_0	σ_a	σ_b	Volume	Photons 10^7
Filter 1	778.8	65.4	64.8	3.39	3.27	54000	9.94
Filter 2	739.9	65.4	64.8	3.39	3.28	52000	9.44
Filter 3	640.5	65.5	64.8	3.03	3.13	38000	6.97
Filter 4	586.5	65.5	64.8	2.97	2.88	32000	5.76
Filter 5	374.5	65.4	64.9	2.68	2.61	16000	3.02
Filter 6	58.11	65.4	64.9	2.49	2.54	2300	0.42

Chapter 4
Monitor Model

The characterization measurements give a good understanding of the system. However, the results are only valid for the system configuration that was tested. To expand the understanding to different configurations, a simulation model was developed.

4.1 The Code

The code was written in MATLAB and it is presented in Appendix A. The model visualizes the image, both in terms of resolution and intensity, at each step throughout the whole system. Figure 4.1 shows a schematic of the different parts of the system and the important parameters. These are also the parameters that the model is based on. The code consists of a main script called "main" that calls for five different functions that modifies the image like each element in the system would do. These five functions are described below.

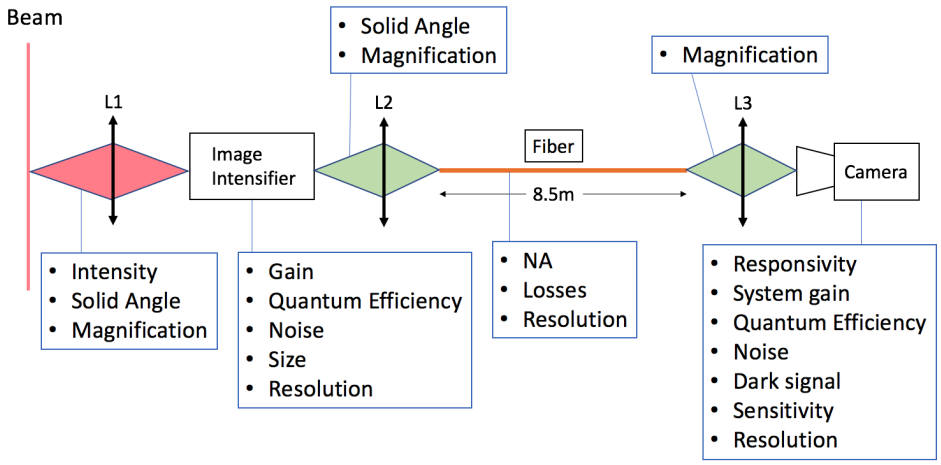

Figure 4.1: A schematic of the NPM, describing the different parts of the system and the parameters that the model is based on.

4.1.1 Light Source

The first function defines the light source. It calculates the number of photons that is generated from one proton pulse. Depending on the first optics the number of photons captured by the lens is calculated. The photons are then given x- and y-coordinates for where in the image intensifier input window, they will end up. The x-coordinate is defined by a uniformly random distribution from zero to the size of the window. The y-coordinate is defined by a normal distribution in the center of the window. The standard deviation is defined by the width of the pulse. This is a variable that can be changed. These coordinates are the outputs of the light source-function. The coordinates are then inserted in a 2 dimensional histogram. The histogram has the same number of bins as the number of channels in the image intensifier. This results in a digitized 2 dimensional matrix of the incoming photons to the image intensifier.

4.1.2 Image Intensifier

This image, or matrix, is the input to the image intensifier-function. In this function a quantum efficiency of the photocathode is defined. The number of photons are converted into a number of electrons defined by a Poisson distribution with $\lambda = \mathrm{N_{ph}} \cdot \mathrm{QE}$, where $\mathrm{N_{ph}}$ is the number of photons for each matrix element and QE is the quantum efficiency. λ is the rate parameter. It is the average number of electrons for a certain number of incoming photons. The number of electrons in each matrix element is then multiplied by the gain factor plus some noise. The noise has been defined as the square root of the value in each element. This can also be changed.

4.1.3 Fiber

Before the fiber-function is called, the optics before the fiber is defined in the main script. The optics has a certain magnification and a solid angle. The solid angle determines the number of photons that are captured from the output of the image intensifier. These two parameters also depend on each other due to the imaging equation. The fiber has a certain number of cores, or channels, with a certain size. In this function the image from the II is mapped onto the new grid of cores in the fiber. For example, if four pixels from the II matrix are imaged onto one core on the fiber, these values get summed up and saved as one element in the new matrix. The magnification will therefore both affect the size of the image in the fiber as well as the intensity. Losses from coupling and attenuation is also multiplied to the matrix. An optional last step can be done to simulate a reduced resolution. The matrix is then convoluted with a normalized Gaussian function with a certain width defining the reduction of resolution.

4.1.4 Camera Input

To define the matrix that represents the image on the camera sensor, the optics between the fiber and the camera is defined in the main script. Since the fiber has a numerical aperture that it emits with and the optics is assumed to have a similar

numerical aperture, all of the light is assumed to be captured by the lens. The solid angle of the lens is therefore not included. The magnification, on the other hand, affects the image. The magnification determines the size of the image on the camera and also how the cores of the fiber maps onto the pixels of the camera. If one core covers 9 pixels, for example, the intensity from this core is placed in the middle pixel of this 3x3 matrix. After that, a convolution with a Gaussian function is performed. The standard deviation is the same as the core width which makes the photons spread out onto all the pixels that the core covers.

4.1.5 Camera

When the image on the sensor is defined, the features of the camera have to be included. The input to this function is the matrix with the number of photons hitting each pixel of the sensor. To convert from photons to electrons the matrix is defined by a Poisson distribution, defined by the quantum efficiency of the sensor. This is done the same as in the image intensifier. After that, dark electrons and a noise are added. The electrons are then multiplied by the system gain, K, to get the number of counts. Read out noise is added. This is now the final image of the whole system.

4.2 Simulations

With this model, the effect of each part of the system can be visualized. This gives a clearer understanding of the impact of the different parameters. To check the reliability of the model, one experimental measurement was imitated and the results were compared. This reveals both the similarities and differences between the model and reality. Furthermore, can the model be used to predict how much the intensity will increase by doing different kinds of improvements.

4.2.1 Beam

Figure 4.2 shows the results of a simulation where the NPM is imaging a beam. The system had similar conditions as in the characterization measurements. The parameters that were chosen are summarized in Table 4.1. The simulation visualizes several features of the NPM. The first subfigure shows the image at the input of the image intensifier. The colorbar is set to a maximum of 2, to make the beam more visible. However, the signal is very low, up to 5 photons per pixel. When this signal has gone through the image intensifier, the number of points are fewer but every point has a higher intensity. The points are hard to see in the figure but they are there. The photocathode reduces the number of photons being detected due to its quantum efficiency, but the photons that are converted into electrons get a high gain through the MCP. When the image has gone through the fiber, each signal has become spatially bigger due to the size of the fiber cores. The signal has also got a lower intensity due to the loss in the optics and in the fiber. When the image arrives at the camera, the intensity has reduced even more and the image is a bit smeared out. The code is written so that the figure of the camera image is zoomed in to the region of interest where the fiber is. In the output of the camera,

the signal is reduced due to its responsivity and noise is also added. To measure the beam width, the image is summed up along the x-axis and a Gaussian fit is performed. The standard deviation of the fitted Gaussian was $\sigma = 3\,\text{mm}$.

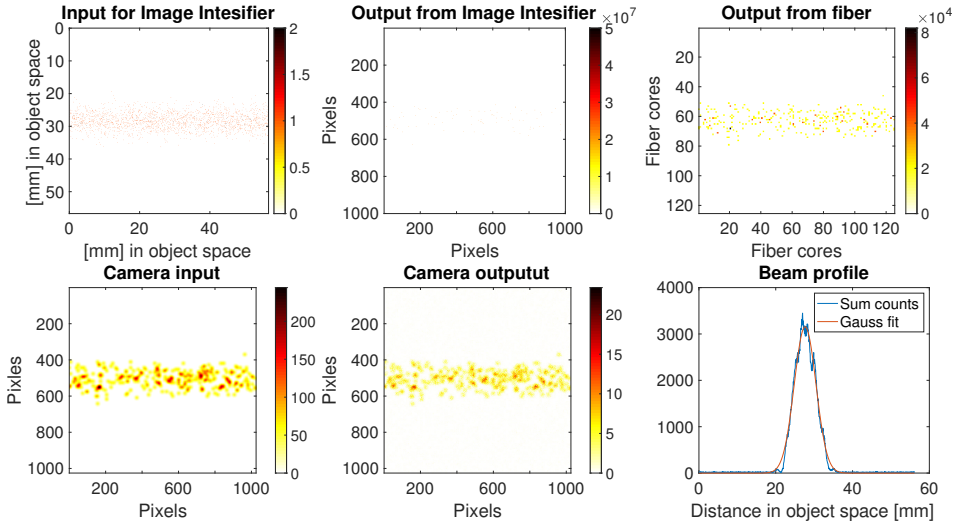

Figure 4.2: Simulation of an image of the beam going through the NPM for similar conditions as in the experimental characterization.

Table 4.1: Parameters that were used in the simulation showed in Figure 4.2.

Light source:	Beam width	5 mm	Fiber:	α	0.0905
	Photons/cm	$2.69 \cdot 10^6$		C	0.58
Lens 1:	M1	0.3		L	8.5
	F1	2	Lens 3:	M3	4
Image Intensifier:	Gain	$2.14 \cdot 10^7$	Camera:	QE	0.52
	QE	5%		K	0.12
Lens 2:	M2	0.23		R	0.062
	Ω	0.0224		Noise	$\sqrt{mean}$

4.2.2 Point source

To investigate the correspondence between the real system and the model, the experimental measurement of a point source detection, described in Section 3.4, was imitated with the simulation. Instead of generating the light source from a beam, the source is defined as an intensity over a certain area at the back of the image intensifier. The intensity was estimated in the measurement and

summarized in Table 3.6. The number of photons for filter 1, 3 and 5 were inserted in the model. The size of the point at the back of the II was not measured but could be estimated from the images. By looking at the mean value of the 20 images taken after the fiber with the first filter, one can see that there is approximately two fiber cores that emit light, see Figure 4.3. The source was therefore defined with an area that maps onto two cores of the fiber. The rest of the system parameters were kept the same as in the first simulation, except the distribution of the light from the fiber output to the camera sensor. This parameter was increased to better match the experimental results. Figure 4.4 shows the results of the simulation with the intensity of filter 5. The source starts at the output of the image intensifier. Two cores of the fiber are illuminated. These are spread out on the camera sensor. A 2D Gaussian fit was performed to the final image. The simulation was then run for the two other filters, 1 and 3. All of the fitting parameters are presented in Table 4.2 together with the experimental results for comparison. The fit of the simulated images has in general a higher peak and the volumes are approximately 50% larger for the simulation. The difference probably comes from the fact that the experimental images are fitted with a Gaussian when they might not be a Gaussian function.

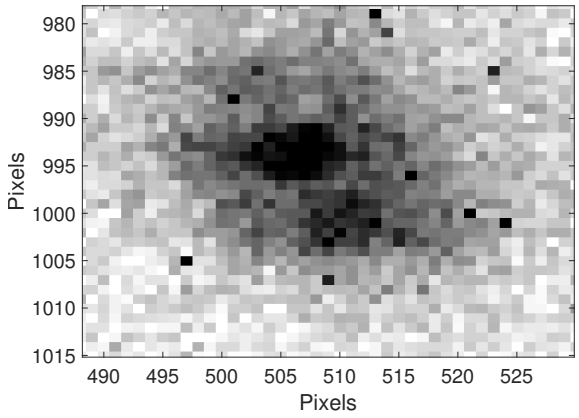

Figure 4.3: Mean value of the 20 images taken with setup 1 (Figure 3.18a), filter 1.

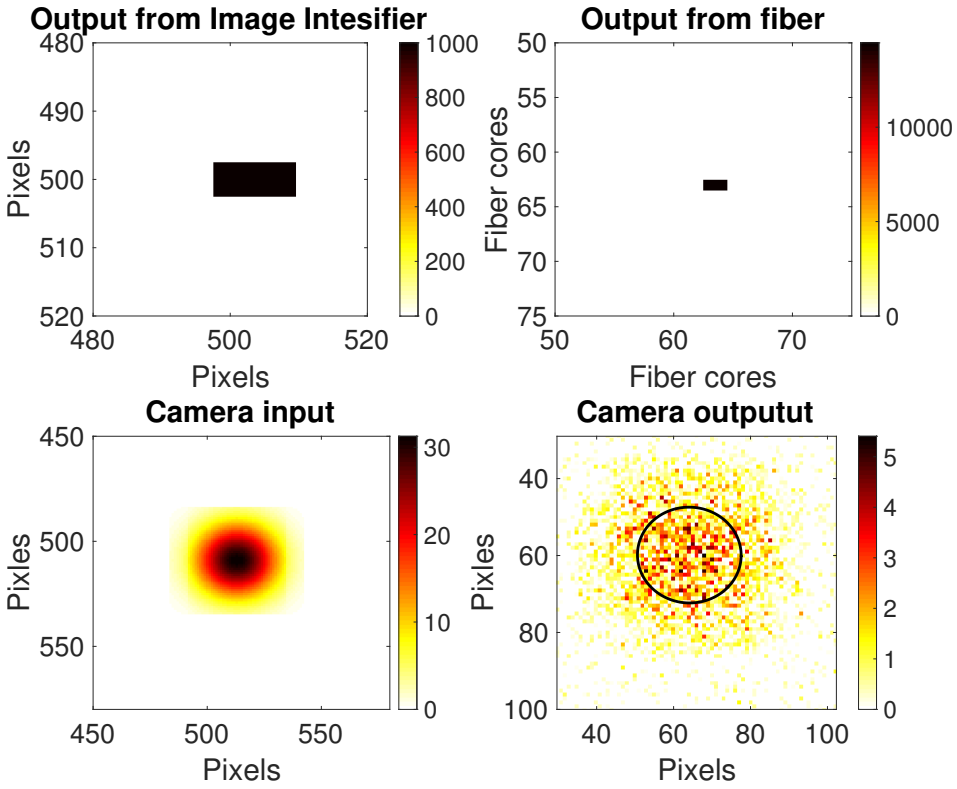

Figure 4.4: Simulation of the measurement done in the characterization of the required gain. The camera output corresponds to the image named filter nr 5 in Figure 3.18a. The black ellipse represents the 2D Gaussian fit.

Table 4.2: 2D Gaussian fit parameters for three different filters. The parameters from the simulations and experiments are shown after each other.

		Peak	σ_a	σ_b	V
Filter 5	Simulation	2.01	13.0	12.7	2094.2
	Experimental	1.27	11.7	13.6	1271.5
Filter 3	Simulation	4.56	13.0	11.8	4413.4
	Experimental	2.57	14.9	12.2	2940.4
Filter 1	Simulation	6.58	12.6	12.2	6347.1
	Experimental	3.44	16.0	11.9	4112.4

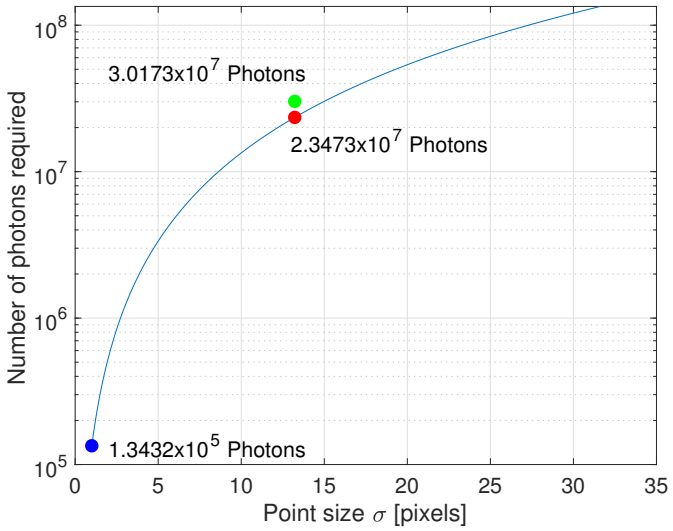

Figure 4.5: Estimated number of required photons as a function of point size at the camera sensor, for a threshold of 23 photons/pixel. The green marker represents the measured value.

4.3 Improvements

Equation (4.1) summarizes the calculations that were included in the model to get the number of required photons, N_{ph}. This is a function of threshold at the camera, N_{th}, standard deviation of the Gaussian distribution, σ, the solid angle of the second lens system, Ω, and the losses of the fiber, $Ce^{-\alpha L}$. The equation indicates how the system can be improved in terms of lowering the required gain. For example, if there is a fiber with lower losses, it would of course improve the system. If a certain number of photons are focused into one pixel instead of four, this would increase the signal per pixel. This is therefore a very efficient way to improve the system. The size of a point source at the sensor, that is σ, changes the number of required photons in a quadratic dependence.

$$N_{ph} = \frac{N_{th} \cdot 2\pi\sigma^2}{\Omega/2\pi \cdot Ce^{-\alpha L}} \tag{4.1}$$

In Figure 4.5, N_{th} is plotted as a function of σ. To be able to compare this estimation with the measurement the threshold was set to the same peak value as measured for filter number 5, $N_{th} = 1.27/R$. A red marker is placed at $\sigma = 13.2$, which is approximately the same as measured with setup 1. For this standard deviation, $2.3473 \cdot 10^7$ photons are required. The result of the measurement was $3.0173 \cdot 10^7$. If the point was focused to 1 pixel instead ($\sigma = 1$), the required number of photons would be $1.3432 \cdot 10^5$, as the blue marker shows. The magnification of the last optical system can therefore be modified to reduce the required gain. The pixel size can also be increased by binning, to increase the signal.

Now the model can be used to see what happens if the magnification of lens 3

is decreased. Figure 4.6 shows the result of the same simulation configuration as in Figure 4.4, but with a magnification of 1 instead of 4 in the last lens system. The intensity of the source is set to be the same as for filter 5, $3.02 \cdot 10^7$ photons. The parameters of the fit is presented in Table 4.3. The parameters from the previous simulation are also included for comparison. The peak of the fit is 15 times higher than for M = 4. This correlates with Equation (4.1), since the magnification has decreased by a factor of 4 and the intensity has a square dependence on σ, it should decrease by a factor of 16. This means that the required gain can be decreased by a factor of approximately 15 if the last lens system has a magnification of 1. The volume on the other hand has decreased a bit. It is because the size of the images were different and this affects the fit.

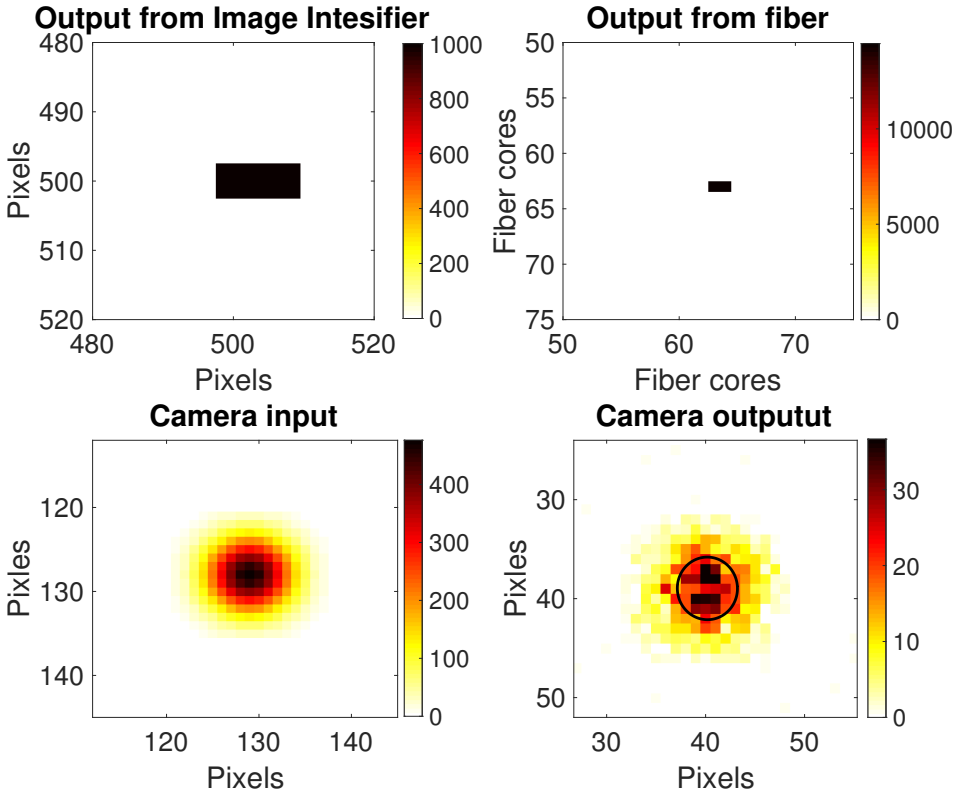

Figure 4.6: The result of the same simulation as in Figure 4.4, but with a magnification of 1 instead of 4 in the last lens system. The black ellipse represents the 2D Gaussian fit.

But what happens with the resolution if the magnification is less than 1? With a magnification of 4, the diameter of one fiber core should be about 7 pixels at the camera. That means that the resolution is limited by the core size and not the pixel size. If the magnification decreases or the pixel size increases so that one fiber core covers one pixel, the resolution will not change significantly. However, the intensity per pixel will increase and the required gain will be lower. The intensity

Table 4.3: Comparison between the 2D Gaussian fit parameters for the simulation with M = 1 and M = 4 in the last lens system.

	Peak	σ_a	σ_b	V
M = 1	30.6	3.10	3.02	1799.0
M = 4	2.01	13.0	12.7	2094.2

can be even higher if the pixel size was larger than the core size, and the resolution does not necessarily has to decrease. The image intensifier generates a distribution of photons for every detected photon. Because it is a distribution, the resolution can be improved with some computational tricks. For instance, the center of mass of the distribution can be found.

Another improvement that can be done, is to decrease the threshold, N_{th}. The camera that was used in this setup has a threshold at 13 photons. There are cameras with lower noise floors than that. One example is the Sony sensor IMX253, that has a noise floor of 2.86 photons [25]. This would decrease the number of required photons by a factor of 4.5 compared to the current camera.

Chapter 5
Discussion

Demonstrating Single Photon Detection

One goal of this thesis is to demonstrate that the Non-Invasive Profile Monitor can perform imaging in single photon counting mode. However, a direct experimental demonstration was not possible to achieve, due to the low gain of the available image intensifier. It was critical to understand the design of the NPM and how it could affect its performance. To this end, a different measurement was performed that could estimate the required gain to make single photon detection possible. The results show that a gain of $3.02 \cdot 10^7$ will give a detectable signal at the camera, with the tested system configuration. This is a quite high number and might not be possible, even with a two-stage amplification. However, the sensitivity can be improved by modifying the parameters of Equation (4.1), as discussed in Chapter 4.

Characteristics of the System

The whole system was experimentally characterized part by part, to find the impact from each component to the final image. The camera has two parameters whose impact on the rest of the system was further investigated. These parameters are the noise floor and the pixel size. The noise floor of the camera defines the threshold of the system. The camera should therefore have a low noise floor. What intensity the camera will receive depends on several things along the rest of the system. The gain of the image intensifier has to compensate for all the losses behind its output. The losses come mainly from the throughput of the optics between the II and the fiber, and from the coupling and attenuation of the fiber. The concept of étendue defines a theoretical limit on how much light that can be captured by the optical system. The étendue is defined by the two surface areas of the image intensifier output and the fiber, and by the numerical aperture of the fiber. If the fiber optical plate has a smaller output area, the magnification can be smaller. This will give a larger throughput according to the formula of the étendue. This must be compared with the losses of having a smaller FOP, so that the gain is larger than the losses.

The optics after the fiber was assumed to have no losses. However, the magnification of the optics was found to play an important role. A smaller magnification give a more intense signal at the camera, because the light is concentrated on fewer

pixels. This effect can also have been applied to the other optical systems. But a smaller magnification would lead to a smaller solid angle, and more losses in lens 1 and 2. Different magnifications for lens 1 were tested in the simulation model. It is not clear if the gain is larger than the loss, with a smaller magnification.

The resolution of the system in the characterized configuration was limited by the size of the fiber cores. This is the case as long as one core is imaged on at least one pixel at the camera sensor. In that case, the pixel size is the limiting factor instead. The resolution is also dependent on the first lens system. This defines how the beam is imaged onto the fiber. If the magnification is very small, the width of the beam could be the same size as one core. But there is no reason to choose such a small magnification, and this is therefore not a problem.

Monitor Model and Improvements

In addition to the experimental characterization, a model of the system was developed. This model can visualize how each component of the system modifies the image of the beam. The model was also compared to one of the experimental results to see if it could be replicated. The model and the experiment got similar results but not the exact same numbers. This might come from the uncertainty in fitting the experimental data to a Gaussian function, when it is not a Gaussian. There could also be losses in the real system that the model does not include. From this model some improvements can be suggested, based on Equation (4.1). The effect of a smaller magnification in the last lens system was simulated. It demonstrated that a decrease in magnification by a factor of 4 gives an improvement in required gain by a factor of 15. The magnification could be even smaller. Another camera sensor was suggested that has a lower noise floor. If this camera is used instead the required gain can decrease by a factor of 4.5. If both these changes are made, the required gain is down to 450 000. An image intensifier with this gain is definitely possible to find.

Conclusions

This thesis has demonstrated the characteristics of each part of the Non-invasive Profile Monitor. A final measurement of the required gain for single photons detection was done. The results show that a gain of $3.02 \cdot 10^7$ gives a detectable signal. The experimental part of this project is complimented with a model that describes how the performance changes when some parameters in the system change. Improvements are suggested based on this model. By doing these modifications the required gain will be down to numbers that image intensifiers on the market have. This proves that the design of this NPM will work in the required condition. This thesis also contains a guideline for designing Fluorescence Profile Monitors in general. The experimental results together with the theory and analysis demonstrate what is possible to achieve. Furthermore, the model can be used for investigating systems' performances with varying design parameters.

Appendix A
Code

Main

```
FS = 18;    %Font size

%% Generate light source
%Define optical system
f_num1 = 2;
M1 = 0.3;
NA1 = M1/(2*f_num1*(M1 + 1));
theta1 = asin(NA1);
T1 = (1 - cos(theta1))/2;
solid_angle1 = T1*2*pi;

%Number of pixels on the sensor
N_pix = [1000 1000];
sensor_size = [0.017 0.017];

object_size = sensor_size./M1;  %Field of view
%Axis in object space
x = linspace(0, object_size(2), N_pix(2))*1e3;
y = linspace(0, object_size(1), N_pix(1))*1e3;

%Get x- and y-coordinates for the incoming photons at the sensor
[x_coord, y_coord, width] = Light_source(N_pix, M1, solid_angle1,
     sensor_size);

N_photons = length(x_coord);    %Number of incoming photons

%generate histogram of the photons
Xedges = 0:N_pix(1);
Yedges = 0:N_pix(2);
f1 = figure;
h = histogram2(y_coord, x_coord, Yedges, Xedges);
image = h.Values;   %matrix with number of photons per pixel
```

```
f2 = figure;
subplot(3, 2, 1)
imagesc(y, x, image);
colorbar
title('Input for Image Intesifier');
xlabel('[mm] in object space');
ylabel('[mm] in object space');
set(gca, 'FontSize', FS);

%% Image intensifier
QE = 0.05;  %quantum efficiency
image_int = intensifier(image, QE);

subplot(3, 2, 2)
imagesc(image_int);
title('Output from Image Intesifier');
colorbar
xlabel('Pixels');
ylabel('Pixels');
set(gca, 'FontSize', FS);


N_photons_in = N_photons*QE;

%% Optical system in front of fiber
FOP_sensor_size = [6.5 6.5]*1e-3;
M_int = FOP_sensor_size./sensor_size;   %magnification through II
fiber_size = [1.5 1.5]*1e-3;

theta = atan(25.4/2/150);
T2 = 1 - cos(theta);
solid_angle2 = T2*2*pi;

%% Image after fiber
%losses in fiber
alpha = 0.0905;
L = 8.5;
C = 0.58;
loss = exp(-alpha*L)*C;

image_fiber = fiber(image_int, solid_angle2, M2, fiber_size,
    FOP_sensor_size, loss);

figure(f2)
subplot(3, 2, 3)
imagesc(image_fiber)
colorbar
title('Output from fiber')
xlabel('Fiber cores');
ylabel('Fiber cores');
set(gca, 'FontSize', FS);
```

```
%% Optical system after fiber
M3 = 1;

image_cam_in = camera_input(image_fiber, M3, fiber_size);

figure(f2)
subplot(3, 2, 4)
imagesc(image_cam_in)
title('Camera input');
colorbar
xlabel('Pixels');
ylabel('Pixles');
set(gca, 'FontSize', FS);

%% From camera input to camera output
image_final = camera(image_cam_in);

figure(f2)
subplot(3, 2, 5)
imagesc(image_final)
colorbar
title('Camera outputut');
xlabel('Pixels');
ylabel('Pixles');
set(gca, 'FontSize', FS);


%% Beam profile
integrated = sum(image_final, 2);
noise_floor = min(integrated);
integrated_minus_noise = integrated - noise_floor;
pixel_size =  5.86e-6;
length_per_pixel = pixel_size./(M1*M_int*M2*M3);
y = (1:s(1))*length_per_pixel(1);

[sigma, mu, A] = mygaussfit(y, integrated_minus_noise);
figure(f2)
subplot(3, 2, 6)
plot(y*1e3, integrated_minus_noise);

title('Beam profile')
xlabel('Distance in object space [mm]')
```

Light source

```
function [x, y, width0] = Light_source(N_pix, M, solid_angle,
sensor_size)
```

```
% Protons per pulse
qe = 1.6e-19;
current = 62.5e-3;
Tpulse = 2.86e-3;
Qpulse = current .* Tpulse;
Nproton = Qpulse ./ qe;

% Vacuum
P0 = 1e-5;      %Pa
nH2cm3 = 6E+23/(8.3145*300)*P0*1e-6;    %cm^3

% H+ - H2 cross section
CSH2 = 1e-18; % cm2

% Number pf photons / pulse / cm
N0 = CSH2 .* Nproton .* nH2cm3

object_size = sensor_size./M;

%Number of photons on sensor
N = round(N0*100*object_size(1)*solid_angle/(4*pi));

width0 = 0.001;                     %width of beam in meter
pixel_size = sensor_size./N_pix;    %pixel size in meter
width = width0*M/pixel_size(1);     %width in number of pixels

x = rand([N 1])*N_pix(2);               %x-coordinate for photons
y = N_pix(1)/2 + randn([N 1])*width/2;  %y-coordinate for photons

end
```

Image Intensifier

```
function image_out = intensifier(image_in, QE)

gain = 600;
%phosphore screen (phototns/electron)
phos = 35;
tot_gain = gain*phos;

%Probability for photon -> electron conversion
transmission = 1;
lambda = image_in*QE*transmission;

%Poisson distribution of electrons
electrons = poissrnd(lambda);

%Amplified electrons
mean_amp_el = electrons*tot_gain;
amp_el = mean_amp_el + randn(size(image_in)).*sqrt(mean_amp_el);
```

```
image_out = amp_el;

end
```

Fiber

```
function image_out = fiber(image_in, solid_angle, M, fiber_size,
FOP_size, loss)

%Captured photons by the lens
image2 = image_in*solid_angle/(2*pi)*loss;

%map image onto fiber matrix
fiber_matrix_dim = [125 125];
fiber_px_size = fiber_size./fiber_matrix_dim;   %12um

image_dim = size(image_in);
image_size = FOP_size*M;
image_px_size = image_size./image_dim;

scale_px = fiber_px_size./image_px_size;
scale_im = image_size./fiber_size;

fiber_matrix = zeros(fiber_matrix_dim);

if scale_im > 1 %fiber smaller than image
    start = (scale_im - 1).*fiber_size/2./image_px_size;
    finish = start + fiber_size./image_px_size;

    row = round(start(1):scale_px(1):finish(1));
    row = [row(1:end-1); row(2:end) - 1];
    col = round(start(2):scale_px(2):finish(2));
    col = [col(1:end-1); col(2:end) - 1];

    for r = 1:fiber_matrix_dim(1)
        for c = 1:fiber_matrix_dim(2)

            matrix_element = image2(row(1, r):row(2, r),
            col(1, c):col(2, c));

            fiber_matrix(r, c) = sum(matrix_element(:));

        end

    end

else    %image smaller than fiber

    row = round(1:scale_px(1):image_dim(1));
```

```
    row_length = length(row) - 1;
    row = [row(1:end-1); row(2:end) - 1];
    col = round(1:scale_px(2):image_dim(2));
    col_length = length(col) - 1;
    col = [col(1:end-1); col(2:end) - 1];

    start = round((1 - scale_im).*fiber_size./(fiber_px_size*2));

    for r = 1:row_length
        for c = 1:col_length

            matrix_element = image2(row(1, r):row(2, r),
            col(1, c):col(2, c));
            fiber_matrix(start(1) + r - 1, start(2) + c - 1)
            = sum(matrix_element(:));

        end

    end

end

image_out = fiber_matrix;

end
```

Camera input

```
function image_out = camera_input(image_in, M, fiber_size)

camera_sensor_dim = [1216 1936];
camera_sensor = zeros(camera_sensor_dim);
pixel_size = 5.86e-6;

fiber_image_dim = size(image_in);

%where does the image start?
image_size = fiber_size*M;
image_size_in_pixels = image_size./pixel_size;

mid = camera_sensor_dim/2;
start = round(mid - image_size_in_pixels./2);

%scale between image pixels and camera pixels
scale = image_size_in_pixels./fiber_image_dim;

%define coordinates where the values go in the sensor
row_end = start(1) + scale(1)*(fiber_image_dim(1) - 1);
row = round(start(1):scale(1):row_end);
```

```
col_end = start(2) + scale(2)*(fiber_image_dim(2) - 1);
col = round(start(2):scale(2):col_end);

if start(1) < 0 || start(2) <0
    I_r = find(row > 0);
    first_r = I_r(1);

    I_c = find(col > 0);
    first_c = I_c(1);

    for r = first_r:(fiber_image_dim(1) - first_r)
        for c = first_c:(fiber_image_dim(2) - first_c)

            camera_sensor(row(r), col(c)) = image_in(r, c);

        end
    end

else

%map matrix
for r = 1:fiber_image_dim(1)
    for c = 1:fiber_image_dim(2)

        camera_sensor(row(r), col(c)) = image_in(r, c);

    end
end

end

sigma = scale/2;

image_out = imgaussfilt(camera_sensor, sigma);  %smear out points
image_out = image_out(start(1):(start(1) +
round(image_size_in_pixels(1))), start(2):(start(2) +
round(image_size_in_pixels(2))));

end
```

Camera

```
function image_out = camera(image_in)

QE = 0.52;        %quantum efficiency  ph -> e
K = 0.12;         %system gain         e  -> DN

%conversion from photons to electrons (Poisson distribution)
lambda = image_in*QE;
electrons = poissrnd(lambda);
```

```
%add dark electrons
dark_el_mean = 0;
dark_el_sigma = 2;
dark_electrons = round(dark_el_mean +
randn(size(image_in))*dark_el_sigma);

total_electrons = electrons + dark_electrons;

%electrons to digital number
DN_mean = total_electrons*K;
DN_sigma = sqrt(DN_mean);

DN = DN_mean + randn(size(image_in)).*DN_sigma;
DN(DN < 0) = 0;

image_out = DN;

end
```

References

[1] Roland Garoby et al. The european spallation source design. *Physica Scripta*, 93(1), 2018.

[2] C. Roose, C. Böhmer, I. Dolenc Kittelmann, A. Jansson, C. Thomas, and A. Källberg, editors. *Development of Non-Invasive Transverse Profile Monitors for the ESS Linac*, Dresden, Germany, 2014. IPAC.

[3] Nist atomic spectra database lines data. `https://physics.nist.gov/cgi-bin/ASD/lines1.pl?spectra=H+I&limits_type=0&low_w=380&upp_w=700&unit=1&de=0&format=0&line_out=0&en_unit=0&output=0&bibrefs=1&page_size=15&show_obs_wl=1&unc_out=1&order_out=0&max_low_enrg=&show_av=3&max_upp_enrg=&tsb_value=0&min_str=&A_out=0&f_out=on&intens_out=on&max_str=&allowed_out=1&min_accur=&min_intens=&conf_out=on&term_out=on&enrg_out=on&J_out=on&g_out=on&submit=Retrieve+Data`. [Online; accessed 18-July-2019].

[4] J. G. Lodge, I. C. Percival, and D. Richards. Semi-empirical cross sections for excitation of hydrogen atoms by protons. *Journal of Physics B: Atomic and Molecular Physics*, 9(2), 1976.

[5] P. Forck, C. Andre, F. Becker, R. Haseitl, and B. Walasek-Höhne, editors. *Beam induced fluorescence profile monitor developments*, number 46, Morschach, Switzerland, September 2010.

[6] ESS Beam Diagnostics. Beam physics, operations beam diagnostics. `https://europeanspallationsource.se/accelerator/beam-physics-operation-beam-diagnostics#beam-diagnostics`. [Online; accessed 27-May-2019].

[7] Michael Lampton. The microchannel image intensifier. *Scientific American*, 245(5), 1981.

[8] Nobel Media AB 2019. The nobel prize in physics 1921. `https://www.nobelprize.org/prizes/physics/1921/summary/`.

[9] Joseph Ladislav Wiza. Microchannel plate detectors. *Nuclear Instruments and Methods*, 167(1-3):587–601, 1979.

[10] Hamamatsu. Image intensifiers brochure, 2016.

[11] R. Holtom, G P Hopkins, and P M Gundry. Surface studies of multialkali antimonide (s20/s25) photocathodes. *Journal of Physics D: Applied Physics*, 12(7), 1979.

[12] Inc. Stanford Computer Optics. Image intensifier: Phosphor screen. `https://stanfordcomputeroptics.com/technology/image-intensifier/phosphor-screen.html`. [Online; accessed 26-June-2019].

[13] Photonis. Image Int. (18mm, Q, FA, Taper, Flying leads), Data Sheet: 183-1476A1, December 2016, Revised May 2018.

[14] William K. Johnston III. The birth of fiberoptics from "light guiding". *Journal of Endourology*, 18(5):425–426, 2004.

[15] Nobel Media AB 2019. The nobel prize in physics 2009. `https://www.nobelprize.org/prizes/physics/2009/summary/`.

[16] B.E.A. Saleh and M.C. Teich. *Fundamentals of Photonics*. John Wiley & Sons, Inc., sedond edition, 2007.

[17] Industrial Fiber Optics. `https://i-fiberoptics.com/fiber-detail-asahi.php?id=3310&sum=162`. [Online; accessed 17-Sep-2019].

[18] EMVA Standard 1288. Standard for characterization of image sensors and cameras, 2016.

[19] R. Javob Baker. *CMOS*. Wiley-Blackwell, third edition, 2010.

[20] Allied Vision. Mako G-234, Data Sheet, [Online; accessed 17-Sep-2019].

[21] John E. Greivenkamp. *Field Guide to Geometrical Optics*. SPIE Field Guides. SPIE - The International Society for Optical Engineering, 2004.

[22] Roland Winston, Juan C. Miñano, and Pablo Benítez. *Nonimaging optics*. Elsevier Academic Press, 2005.

[23] Caroline Boudoux. *Fundamentals of Biomedical Optics*. Pollux, first edition, 2016.

[24] Thorlabs. `https://www.thorlabs.com/thorproduct.cfm?partnumber=MCWHF2`. [Online; accessed 17-Sep-2019].

[25] Basler. Emva data overview - monochrome area scan cameras, 2019.